ACS Sustainable Chemistry & Engineering

pubs.acs.org/journal/ascecg

Research Article

Switchable Behavior of Ru−TiO_2 Catalysts in HMF Conversion

Babar Amin, Jaroslav Aubrecht,* Oleg Kikhtyanin, Evgeniya Grechman, Gustavo Andrade Silva Alves, Alberto Tampieri, Karin Föttinger, Marcin Jędrzejczyk, Agnieszka M. Ruppert, Francisco Ruiz-Zepeda, and David Kubička

Cite This: *ACS Sustainable Chem. Eng.* 2025, 13, 11652−11667

Read Online

ACCESS | Metrics & More | Article Recommendations | Supporting Information

ABSTRACT: 5-Hydroxymethylfurfural (HMF) is a platform chemical that can be catalytically valorized into high-value-added chemicals. Despite the extensive use of titania-supported metal catalysts in HMF conversion, the specific influence of the TiO_2 support on the formation of metal active sites, their dispersion, and their role in HMF conversion is not addressed sufficiently. In this work, we investigated five TiO_2 supports, four anatase- and one rutile-dominant, varying in surface area and acidity, which were loaded with 1 wt % Ru using $RuCl_3$. Characterization results revealed that the Ru environment, charge distribution, and surface features (transition from Ru−Cl to Ru−O species) varied depending on the TiO_2 support used. Their catalytic performance was assessed in HMF hydrogenation. Despite identical Ru loadings, the Ru/TiO_2 catalysts exhibited remarkably different catalytic activities and selectivity. High-surface-area anatase TiO_2 led to the formation of smaller Ru particles and supported the conversion of HMF to 5-methylfurfural. In contrast, lower surface area anatase and rutile supports favored the formation of larger Ru particles and redirected the reaction course from 5-MF toward the hydrogenation route, yielding primarily 2,5-bis(hydroxymethyl)furan. This study revealed the switchable behavior of Ru/TiO_2 catalysts and exposed the critical role of TiO_2 structural and morphological features for reaction pathways in HMF valorization over Ru/TiO_2. These insights provide a refined framework for the rational design of oxide-supported catalysts tailored for the selective conversion of biomass.

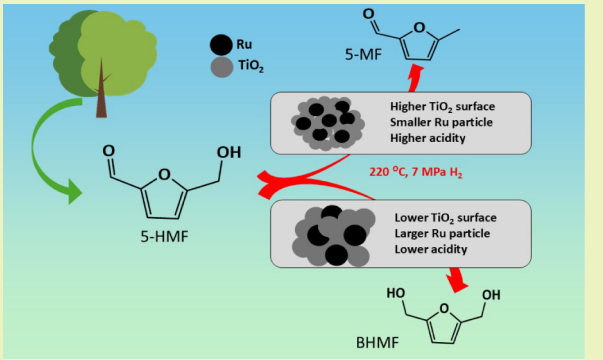

KEYWORDS: *Ru/TiO_2 catalysts, hydrogenation, hydrogenolysis, 5-hydroxymethylfurfural, 5-methylfurfural, 2,5-bis(hydroxymethyl)furan*

1. INTRODUCTION

The utilization of biomass has attracted the attention of researchers to replace diminishing fossil resources for the production of energy and chemicals. Typical examples of biomass-derived compounds are furanics such as 5-hydroxymethylfurfural (HMF). The direct conversion of fructose to HMF occurs via an acid-catalyzed dehydration reaction.[1,2] HMF contains three functional groups (C=C, C−O, and C=O), making it a versatile compound with high potential for synthesizing value-added chemicals, such as 5-methylfurfural (5-MF), 2,5-bis(hydroxymethyl)furan (BHMF), 2,5-bis(hydroxymethyl)tetrahydrofuran (BHMTHF), 2,5-dimethylfuran (DMF), 2,5-furandicarboxylic acid (FDCA), etc. Both 5-MF and DMF are valuable as biofuel additives due to their high energy density and compatibility with the existing fuel systems.[3,4] BHMF, a diol, serves as a key intermediate in the synthesis of biobased polymers, particularly BMHF-derived polyesters.[5] FDCA is used as a renewable alternative to terephthalic acid in the production of sustainable polyesters such as PEF.[6]

Significant research has been focused on the conversion of HMF into value-added chemicals via hydrogenation and hydrogenolysis pathways.[7] Ru-based catalysts are often used for HMF conversion due to their high activity associated with the formation of small Ru nanoparticles with a size of 1−2 nm along with strong metal−support interaction.[7−9] A variety of supports, such as activated carbon materials and metal oxides (e.g., TiO_2, Al_2O_3, ZrO_2), have been explored to optimize the catalytic activity and selectivity of Ru catalysts in different reactions.[10,11] The performance of Ru catalysts is significantly influenced by the nature of the support, which affects Ru dispersion, its electronic properties, and the stability of the catalyst.[12] Among them, the Ru-TiO_2 catalyst has been reported to exhibit the highest activity, attributed to the TiO_2 acidic sites,

Received: May 20, 2025
Revised: June 30, 2025
Accepted: July 11, 2025
Published: July 18, 2025

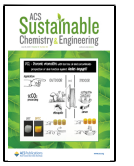

https://doi.org/10.1021/acssuschemeng.5c04908
ACS Sustainable Chem. Eng. 2025, 13, 11652−11667

which enhance HMF adsorption and facilitate the hydrogenation step.[8,9] These sites are predominantly Lewis acid sites and provide titania with its intrinsic activity. We have reported that HMF undergoes disproportionation to 2,5-diformylfuran (2,5-DFF) and 5-MF over these Lewis acid sites.[13]

Ru-based catalysts were used in HMF conversion, resulting in the formation of BHMF followed by its hydrogenation to BHMTHF. Recently, Kashyap et al. highlighted the role of Ru particle size and reduction temperature, which influenced the performance of Ru/TiO_2 catalysts in HMF conversion. Under optimized conditions, they achieved 98% of BHMF yield and demonstrated the good recyclability of the catalyst in several reaction cycles.[7] Rodríguez-Padrón et al. compared the performance of different Ru-based catalysts in HMF hydrogenation, and the use of Ru/CeO_2 favored 94% BHMF yield while Ru/Mg−Zr led to BHMTHF formation.[14] Fulignati et al. reported BHMF yields of 87.9% in a continuous-flow reactor using Ru/C, but the catalyst has deactivated because of humins formation;[15] however, the nature of support in Ru dispersion was not discussed. In addition to BHMF, HMF can also be directly hydrogenolyzed into 5-MF. This approach was previously reported by Dong et al.,[16] who demonstrated a selective HMF conversion with up to 83% selectivity of 5-MF using Au-based catalysts. However, their study did not look into the role of the support material in influencing Au dispersion and catalytic performance. Similarly, Pt/Nb_2O_3 single-atom catalysts were prepared and tested in HMF to 5-MF formation.[17]

To load Ru on a support, various Ru precursors such as $RuCl_3 \cdot xH_2O$, $Ru(acac)_3$, or $Ru(NO)(NO_3)_3$ are often used.[7,18−20] Among them, $RuCl_3$ is preferred owing to its ease of use and low price. Moreover, it has been shown to afford a higher number of available Ru active sites than other Ru precursors.[7] Nevertheless, the Ru−support interaction might vary depending on the surface properties of titania. This essential interaction contributes to several critical factors, including (i) the final size of Ru particles, (ii) their reducibility and charge distribution, and (iii) the formation of active sites.[21,22] However, the nature and specific role of the titania surface and structural composition in the formation of Ru species and their effect on HMF reaction pathways have not been sufficiently addressed in the literature.

This study reports on the influence of TiO_2 supports with varying surface areas and phase compositions on the formation of Ru nanoparticles, their structure, local environment, and their activity and selectivity in HMF hydrogenation. A series of four commercial supports and one laboratory-designed anatase TiO_2 loaded with 1 wt % Ru were prepared and comprehensively characterized to gain insights into the size and environment of the Ru species using advanced spectroscopic methods, including X-ray photoelectron spectroscopy (XPS), time-of-flight secondary ion mass spectrometry (TOF-SIMS), Fourier transform infrared spectra with CO adsorption (CO-FTIR), and transmission electron microscopy (TEM). This enabled a detailed understanding of Ru dispersion and its oxidation state and particle size, which are critical parameters that govern different HMF catalytic activities and contribute to a rational design of more efficient Ru-based catalysts.

2. EXPERIMENTAL PART

2.1. Materials. In this work, four commercial TiO_2 samples were used as supports and further denoted as TiO_2-S (NorPro Saint-Gobain Company, 99.3%), TiO_2-A (Merck Company, 99.8%), TiO_2-R (Aldrich Company, 99.9%), and TiO_2-T (Merck Company, 99.5%). Additionally, a lab-made TiO_2-B sample was prepared using titanium(IV) *tert*-butoxide (TBT, Merck Company, USA, purity 97%) as a precursor. To prepare the Ru catalysts, $RuCl_3$ (45−55% Ru, Merck Company) was used. For catalytic experiments, 5-hydroxymethylfurfural (HMF >99%, AVA Biochem, Switzerland), tetrahydrofuran as a solvent (THF, ≥99%, Sigma-Aldrich), and *n*-dodecane as an internal standard (≥99%, Sigma-Aldrich) were used.

2.2. Support and Catalyst Synthesis. Laboratory-prepared titania named TiO_2-B was prepared by hydrolysis of TBT. Typically, 30 mL of TBT was dissolved in 150 mL of dry ethanol and stirred for 1 h. Then, 150 mL of deionized (DI) water was added, and the resulting slurry was stirred at room temperature (RT) for 4 h, followed by aging for 48 h at RT, filtration of the precipitate, washing with DI water, drying at 80 °C for 6 h, and calcination at 400 °C for 4 h.

To prepare Ru-containing catalysts, $RuCl_3$ was loaded to get 1 wt % Ru on TiO_2-S, TiO_2-T, TiO_2-A, TiO_2-R, and TiO_2-B using a wet impregnation method. All TiO_2 supports were dried in air at 150 °C for 2 h. To obtain the targeted Ru loading, the calculated amount (0.103 g) of $RuCl_3$ was dissolved in 50 mL DI water with the help of sonication and intensive stirring at RT until a clear black brownish solution was formed, and then the calculated amount of a dried TiO_2 support (4.9 g) was added to the solution. The suspension was stirred at RT for 1 h at 300 rpm, and then, water was removed by a rotary evaporator at 80 °C. The obtained solid was dried in an oven at 100 °C for 5 h.

For characterization purposes, all catalysts were prereduced in an autoclave in the flow of H_2 at 400 °C for 30 min, and the resulting samples were denoted as $1Ru/TiO_2$-x-Red.

2.2.1. Catalyst Testing. All prepared catalysts were tested in 5-hydroxymethylfurfural (HMF) hydrogenation in a stirred batch reactor (300 mL Parr autoclave). Initially, a Ru/TiO_2 catalyst (0.5 g) was reduced *in situ* at 400 °C in the autoclave for 1 h under the flow of H_2 at atmospheric pressure. Then, the autoclave was cooled to RT under N_2 flow, and a mixture consisting of 3 g of HMF dissolved in 90 g of THF solvent with 1 g of *n*-dodecane as an internal standard was loaded. The autoclave was flushed with H_2 for 20 min at 200 rpm. Then, the temperature was increased to 220 °C, followed by fixing the H_2 pressure at 7.0 MPa and stirring speed at 600 rpm (reaction time = 0). These reaction conditions were kept for 3 h, during which liquid samples of the reaction mixture were periodically taken at specific times. The withdrawn samples were analyzed using an Agilent 7820A GC unit equipped with an HP-5 column and an FID detector.

HMF conversion (eq 1) and product yields (eq 2) were calculated by the following equations:

$$x_{\mathrm{HMF}}\ (\%) = \frac{n_{\mathrm{HMF}(t=0)} - n_{\mathrm{HMF}(t=x)}}{n_{\mathrm{HMF}\ (t=0)}} \times 100 \tag{1}$$

$$\mathrm{Yield}_{\mathrm{Z}}(\%) = \frac{n_{\mathrm{product\ Z}\ (t=x)}}{n_{\mathrm{HMF}\ (t=0)}} \times 100 \tag{2}$$

where x_{HMF} is the conversion of HMF, n_{HMF} represents HMF moles, $t = 0$ is the time at the beginning of each experiment, $t = x$ is the sampling time, and $n_{\mathrm{product\ Z}}$ represents the moles of product Z. The initial reaction rate (r) at 5 min was calculated using eq 3:

$$r = \frac{\mathrm{nHMF\ converted}}{t \times m} \tag{3}$$

where n is HMF moles converted, t is time in seconds, and m is the catalyst mass; the unit of r is $\mathrm{mol \cdot s^{-1} \cdot g^{-1}}$.

2.2.2. Characterization of Catalysts. The chemical composition of the prepared catalysts was determined by X-ray fluorescence (XRF) using an Axios spectrometer equipped with a rhodium lamp.

The XRD patterns of the prepared samples were recorded in the range of $2\theta = 5-80°$ using a PANanalytical X'Pert3 Powder diffractometer and Cu Kα radiation for the determination of phase composition and the mean crystallite size of pure supports. The reflections at $2\theta = 25.3°$ and 27.5° were taken for the calculation of mean crystallite size in the case of anatase and rutile phases, respectively, using the Scherrer equation.

Fourier transform infrared spectra (FTIR) of pure TiO_2 supports were recorded on a Bruker Alpha II FTIR spectrometer equipped with

https://doi.org/10.1021/acssuschemeng.5c04908
ACS Sustainable Chem. Eng. 2025, 13, 11652−11667

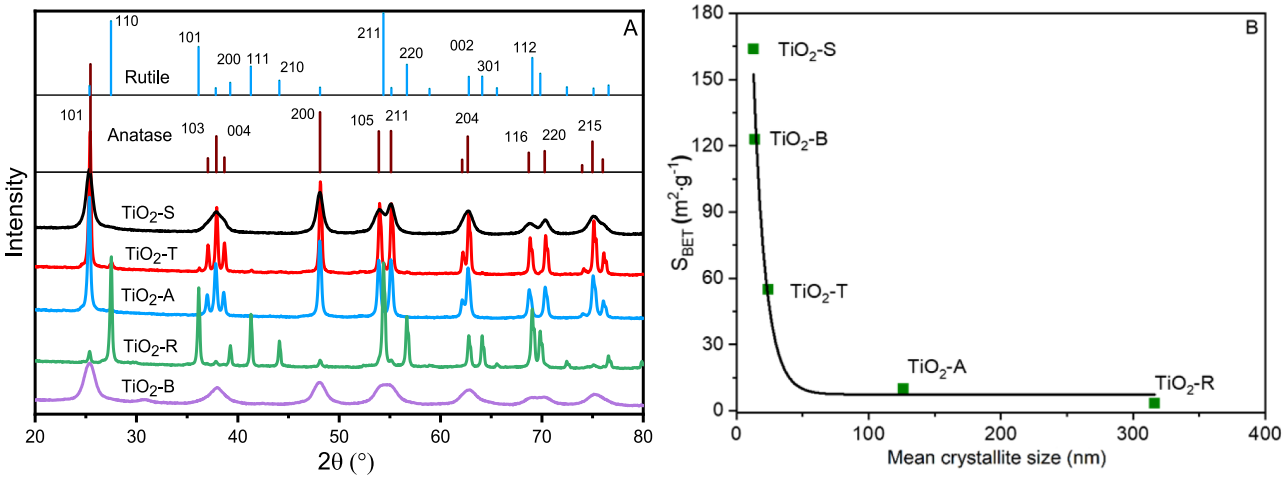

Figure 1. XRD pattern of titania supports (A) and the correlation between the surface area and the mean crystallite size (B).

an attenuated total reflection (ATR) platinum diamond in the region of 450 to 4000 cm^{-1}.

The specific surface area was measured using a Coulter SA 3100 instrument (Beckman Coulter). Both adsorption and desorption isotherms were collected at a relative pressure in the range of 0−0.99 at a temperature of −196 °C. The total pore volume was determined from the quantity of adsorbed nitrogen at a relative pressure close to 1. Pore size distribution was calculated from the desorption isotherms based on the Barret−Joyner−Halenda model.

H_2 temperature-programmed reduction (H_2-TPR) was performed using an AMI-300 catalyst characterization system that was equipped with a thermal conductivity detector (TCD). Approximately 50 mg of a catalyst was placed in a U-shaped quartz reactor, then purged with argon at 25 cm^3/min, was heated up to 150 °C at a heating rate of 10 °C/min, and kept at 150 °C for 60 min. Then, the temperature was decreased to 70 °C, 10% H_2/Ar mixture was introduced, and the temperature was increased from 70 to 700 °C with a heating rate of 10 °C/min. The degree of reduction of Ru in the samples was calculated according to eq 4

$$\text{degree of reduction (\%)} = \frac{\text{H}_2\text{ uptake} \times M_{\text{Ru}}}{\text{wRu} \times \text{stoichiometric factor} \times 100} \quad (4)$$

where H_2 uptake is the amount of H_2 consumed in μmol·g^{-1}, M_{Ru} is atomic mass of Ru, w_{Ru} is Ru loading (wt %), and the stoichiometric factor of 1.5 is the amount of H_2 moles required to reduce 1 mol of $RuCl_3$.

Ru dispersion D_{Ru} was calculated using TEM particle size considering the hcp structure of Ru using eq 5 from ref 23.

$$\begin{aligned} D_{\text{Ru}} &= \frac{N_{\text{surface Ru}}}{N_{\text{total Ru}}} \times 100 \\ &= \frac{f \times N_{\text{total Ru}}}{\frac{V_{\text{particle}}}{V_{\text{Ru,hcp}}}} \times 100 \\ &= \frac{\frac{3}{d/a} \times N_{\text{total Ru}}}{\frac{\frac{4}{3}(\pi . r^3)}{0.0224}} \times 100 \end{aligned} \quad (5)$$

where $N_{\text{surface Ru}}$ is the number of Ru atoms on the surface, $N_{\text{total Ru}}$ is the total number of Ru atoms, $f = \frac{3}{d/a}$ is an empirical factor for the available surface atom in the hcp structure, d is particles' diameter, a and c are hcp unit cell parameters (a = 2.705 Å, c = 4.281 Å), and r is the determined radius of Ru hcp particles, $V_{\text{particle}}$is the volume of particles, and $V_{\text{Ru,hcp}}$ is the atomic volume of hcp Ru (calculated using $\frac{a^2.c.\sqrt{3}}{2}$ equal to 0.0224 nm^3).

The specific surface area of Ru (S_{Ru}) was calculated using eq 6 from ref 23.

$$S_{\text{Ru}} = N_{\text{total Ru}} \times D_{\text{Ru}} \times A_{\text{Ru}} = \frac{w_{\text{Ru}}}{M_{\text{Ru}}} \times N_{\text{A}} \times D_{\text{Ru}} \times A_{\text{Ru}} \quad (6)$$

where $N_{\text{total Ru}}$ is the total number of Ru atoms, D_{Ru} is Ru dispersion, A_{Ru} is the Ru atomic surface area (0.0635 nm^2), w_{Ru} is the mass fraction of Ru, M_{Ru} is the molar mass of Ru, and N_{A} is the Avogadro number.

The properties of the TiO_2 surface were investigated using isopropanol-TPD (IPA-TPD). Before the experiments, all pure supports were pretreated at 150 °C in air. Isopropyl alcohol (99%, PENTA, s.r.o.) was heated to 30 °C and bubbled with a N_2 (99.9%) flow. The flow of isopropanol/N_2 passed through the pretreated sample (0.2 g) in a chamber heated to 80 °C for 2 h. The sample was then transferred into a Quantachrome ASiQ sorption system and treated by a N_2 flow (40 cm^3/min) at 80 °C for 12 h, followed by an increase of the temperature to 650 °C with a ramp of 20 °C/min. The effluents were monitored by a mass spectrometer (Pfeiffer PrismaPlus MS).

Time-of-flight secondary ion mass spectrometry (ToF-SIMS) was performed to analyze the surface composition of the catalysts using a TOF-SIMS IV instrument (ION-TOF GmbH, Germany) equipped with a 25 kV Bi_3^+ pulsed ion gun. Prior to measurement, samples were gently pelletized and attached to a sample holder with an adhesive tape. At least three spectra from different locations were collected for each sample. The analyzed area corresponded to a square of 500 μm × 500 μm. The intensities of all ions were normalized to the total sum of ions.

Fourier transform infrared (FTIR) spectra of adsorbed CO were collected on a Nicolet 6700 spectrometer equipped with a liquid-nitrogen-cooled MCT detector and a DRIFT environmental chamber (Specac Ltd., England). A catalyst was placed in a sample holder, reduced in situ at 400 °C in a 5% H_2/Ar flow (20 cm^3/min) for 1 h, and cooled to RT in an argon flow (20 cm^3/min) before recording the background spectrum. CO adsorptions were carried out in a 5% CO/Ar flow (20 cm^3/min) for 20 min at RT. Excessive CO was then eluted from the chamber in an Ar flow (20 cm^3/min) for 20 min at RT. All spectra were recorded with a resolution of 4 cm^{-1}, collecting 64 scans.

Scanning Transmission Electron Microscopy (STEM) imaging of reduced catalysts was carried out using a JEOL ARM 200CF microscope operated at 80 kV. For the particle size distribution diagram, 100 particles were evaluated in the case of 1Ru/TiO_2-T-red, 1Ru/TiO_2-A-red, and 1Ru/TiO_2-R-red (100), while 54 and 50 particles were considered in the case of 1Ru/TiO_2-B-red and 1Ru/TiO_2-S-red, respectively.

The XPS study was performed using a SPECS u-Focus system (AlKα source, Phoibos 150 WAL detector). Data evaluation was carried out with CasaXPS software.[24] The peaks were fitted with Gauss−Lorentz (GL) sum functions and a Shirley background. All spectra were calibrated for the main component of adventitious carbon at 284.8 eV.

https://doi.org/10.1021/acssuschemeng.5c04908
ACS Sustainable Chem. Eng. 2025, 13, 11652−11667

For the quantification of surface species, the areas of Ru $3d_{5/2}$, Cl 2p, and Ti 2p were considered, along with the respective Relative Sensitivity Factors (RSF) of 7.39, 2.29, and 7.81. Further analysis of the samples was done after treatment under a 50% H_2 flow in He at 400 °C for 30 min.

The thermogravimetry analysis (TGA-MS) of spent catalysts was performed using a Setaram Evo TGA/DTA Instruments and treating 0.03 g of sample in an air atmosphere from RT to 900 °C at a rate of 10 °C·min^{-1}.

The elemental analysis (C, H, S, and N) of spent samples was carried out using an Elementar vario EL cube instrument (Elementar Co.). The accuracy of the method was determined by the simultaneous analysis of a standard 4-amino-benzenesulfonic acid (5 mg) in the module.

The density of carbon (n_C) on the surface was calculated according to eq 7:

$$n_C = \frac{w_c}{S_{BET}} \quad (7)$$

where w_C is the determined C content using elemental organic analysis and S_{BET} is the surface area of the catalysts.

3. RESULTS AND DISCUSSION

3.1. Characterization of Titania Materials. Figure 1A depicts the XRD patterns of all five TiO_2 supports used in this study. Three titania crystalline phases, i.e., anatase, rutile, and brookite, can be present in the samples.[25] Three samples (TiO_2-S, TiO_2-A, and TiO_2-B) represented the anatase phase (assigned to JCPDS 96-960-8214), while TiO_2-R contained 96% of the rutile phase (JCPDS 01-084-1286). The TiO_2-T sample was a mixture of anatase and rutile phases with a ratio of 86:14 according to SemiQuant analysis based on observed reflections. To distinguish between these two phases, specific reflections at $2\theta = 25.3°$ attributed to the (101) crystalline plane of the anatase framework and at $2\theta = 27.5°$ attributed to the (110) crystalline plane of the rutile framework were used. The presence of brookite was ruled out in each sample. The mean size of crystallites in the TiO_2 samples was significantly different in the range 13−316 nm (Table 1). This difference was directly reflected in the BET surface area values of the supports determined by N_2 physisorption (Table 1 and Figure 1B). The BET surface area decreased from about 160 to 4 $m^2 \cdot g^{-1}$ in the following order: TiO_2-S > TiO_2-B > TiO_2-T > TiO_2-A > TiO_2-R. Moreover, the XRD patterns of titania samples with the largest BET surface area showed the broadening of XRD reflections, thus evidencing not only the small size of TiO_2 particles but also their partial polycrystalline morphology, which was additionally confirmed by TEM (Figure S1A−C). The evaluated TiO_2 particle sizes using TEM images (Table 1) were correlated with the XRD mean crystallite size. ATR-FTIR was further used to characterize the structure of the TiO_2 samples (Figure S2). An intense band at 400−500 cm^{-1} corresponded to Ti−O−Ti bending vibration and Ti−O vibrational mode in the TiO_2 lattice. A clear band at about 450 cm^{-1} proved the presence of rutile phase in TiO_2-T and TiO_2-R samples.[26] The FTIR spectra of TiO_2-S, TiO_2-B, and TiO_2-A were similar due to the sole existence of the anatase phase in these samples, while the spectra of TiO_2-R and TiO_2-T differed in the region of 400−500 cm^{-1} due to the presence of the rutile phase.

Table 1. Strural and Textural Properties of Titania Support

Material	S_{BET} ($m^2 \cdot g^{-1}$)	d_{TiO2} (nm)[a]	anatase/rutile (%)	d_{TiO2} (nm)[b]
TiO_2-S	164	13[bc]	100/0	9 ± 1.5
TiO_2-T	55	24[b], 22[d]	86/14	20 ± 5
TiO_2-A	10	126[b]	100/0	115 ± 12
TiO_2-R	3.5	316[c]	6/94	400 ± 25
TiO_2-B	123	14[b]	100/0	12 ± 2.2

[a]TiO_2 mean crystallite size determined by XRD. [b]Anatase (101). [c]Rutile (110). [d]TiO_2 particle size determined by TEM.

The IPA-TPD method was employed to probe the surface of the TiO_2 samples. IPA can be adsorbed on both titanyl (Ti−OH) and Lewis acid sites (Ti^{IV}) on a TiO_2 surface.[13,27] Previously, it has been reported that adsorbed IPA on TiO_2 produces propene at temperatures above 300 °C, and this reaction happens on Lewis acid sites through Hoffman elimination,[28] while the presence of basic sites is responsible for the formation of acetone and isopropyl ether.[13] Based on pyridine-FTIR, we have concluded that titania pretreated at T > 150 °C in H_2, i.e., at reaction conditions, possessed mostly Lewis acid sites.[13] From our previous investigation, IPA can adsorb on Lewis acid sites, followed by dehydration to produce propene.[13] Both propene (m/z 41) and acetone (m/z 58) were detected in MS-TPD profiles upon IPA interaction with TiO_2 samples (Figure S3A,B). Nevertheless, the intensity of the propene peak originating from supports with high surface area was about 2 orders of magnitude larger than that of the acetone peak, indicating the presence of rather acid than base sites. The number of both acid and basic sites evaluated from the peak area of released propene and acetone, respectively, correlated with the surface area of the pure TiO_2 materials (Figure 2A,B). This was in line with our previous observations,[13] when the acidity of titania samples determined by pyridine-TPD increased with their increasing surface area values. The ratio between the peak area of propene and acetone exhibited a decreasing trend in the following order: TiO_2-B (13), TiO_2-S (11), TiO_2-T (10), TiO_2-R (1), and TiO_2-A (0.5).

3.2. Interaction of Ru with Titania Support. To prepare Ru/TiO_2 catalysts, all reported TiO_2 supports were impregnated to get 1 wt % Ru using $RuCl_3$ as a precursor. Table 2 presents actual Ru and Cl loadings in the samples determined by XRF. For all the catalysts, the Ru content was 0.93 ± 0.04 wt %, thus matching the targeted value, while the Cl content originating from $RuCl_3$ significantly differed. A theoretical Cl/Ru atomic ratio should be 3. Nevertheless, the actual Cl/Ru values in the prepared samples varied from 3.2 to 0.8 (Table 2). The calculated Cl/Ru ratio correlated well with the titania BET surface area: the larger the surface area, the higher the Cl/Ru ratio in the prepared samples (Figure 3). Anatase-type TiO_2 has a higher surface area than rutile-type TiO_2, so more residual Cl was detected in the anatase-based catalysts.

The surface area and phase composition of Ru/TiO_2 catalysts were analyzed using N_2 physisorption and XRD, respectively. After Ru loading, the surface areas of Ru/TiO_2-S and Ru/TiO_2-B slightly decreased, which is the result of the surface constraint due to the deposition of $RuOCl_x$ species and partial pore blockage (Table 2) as well as experimental error. In contrast, there was no significant change in the surface area of Ru/TiO_2-T and Ru/TiO_2-A, while an increase in the surface area of Ru/TiO_2-R was observed. In the XRD patterns, no distinct reflection corresponding to Ru crystallite planes was observed, which could be ascribed to the small size of Ru particles or to low Ru content, which was below the XRD detection limit (Figure S4).

To investigate the chemical state of catalysts' surface, TOF-SIMS (Figure 4) and XPS (Figure 5) analyses were performed. The intensities of Ru ion signals were the highest for 1Ru/TiO_2-A and 1Ru/TiO_2-R samples (Figure 4A). At the same time, Ti ion signals recorded for both catalysts were the lowest. This

https://doi.org/10.1021/acssuschemeng.5c04908
ACS Sustainable Chem. Eng. 2025, 13, 11652−11667

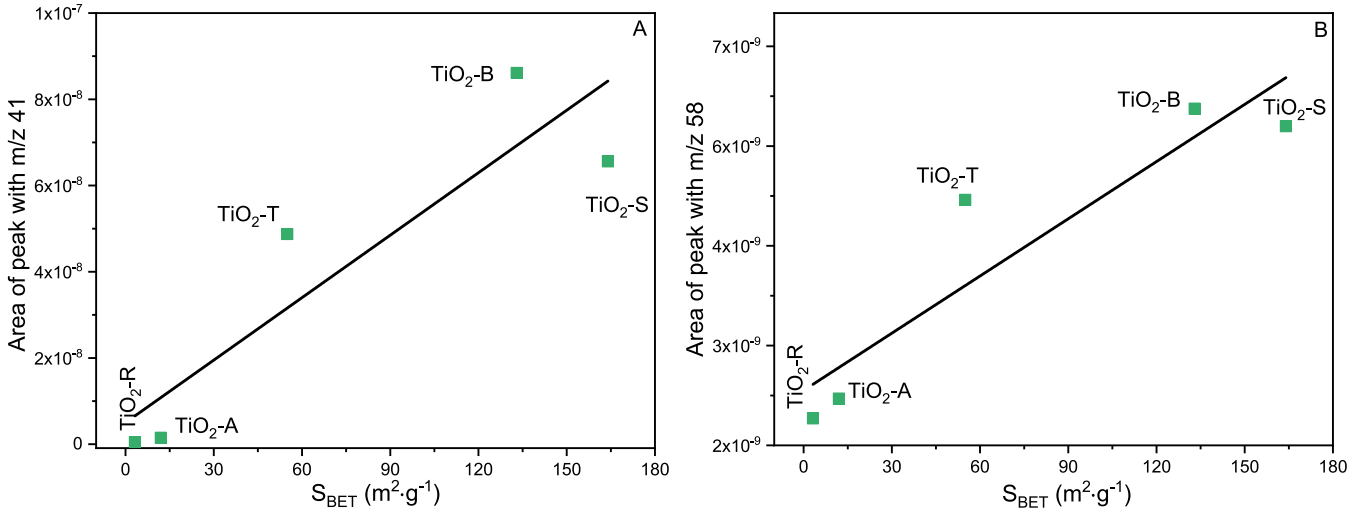

Figure 2. Correlation between the peak area for propene (the MS signal with $m/z = 41$) (A) and acetone ($m/z = 58$) (B) and the BET surface area of TiO_2.

Table 2. Bulk and Surface Chemical Composition of the Prepared Catalysts

Catalyst	w_{Ru} (wt %)	w_{Cl} (wt %)	n_{Cl}/n_{Ru} bulk[a]	S_{BET} ($m^2 \cdot g^{-1}$)	Cl/Ru TOF-SIMS[b]	n_{Cl}/n_{Ru} surface[c]
1Ru/TiO_2-S	0.93	1.0	3.2	154	0.1	0.4
1Ru/TiO_2-T	0.93	0.8	2.5	56	0.1	0.4
1Ru/TiO_2-A	0.93	0.5	1.7	12	0.1	0.2
1Ru/TiO_2-R	0.97	0.3	0.8	8	0.3	0.2
1Ru/TiO_2-B	0.93	0.9	2.7	106	0.1	0.4

[a]By XRF. [b]By TOF-SIMS, the ratio of Cl^- ions with Ru^+ ions. [c]XPS Cl/Ru surface atomic ratio.

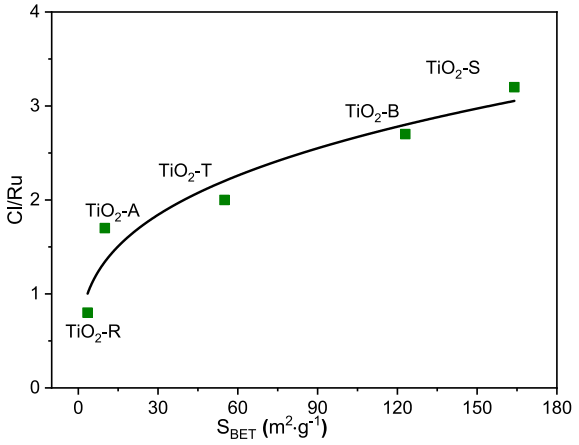

Figure 3. Correlation between Cl/Ru atomic ratio in the Ru/TiO_2 samples and the BET surface area of pure TiO_2 supports.

indicated the limited accessibility of Ti atoms after the deposition of Ru species, which was a consequence of the low specific surface area of the TiO_2-A and TiO_2-R supports. In contrast, the spectra of 1Ru/TiO_2-S, 1Ru/TiO_2-B, and 1Ru/TiO_2-T revealed the lowest intensity of signals from Ru ions and the highest intensity of signals from Ti ions.

Interestingly, various Ru/Cl/O fragments were detected on the catalyst surface, suggesting the formation of diverse Ru species (Figure 4B). While the Cl and RuO_2 fragment signals were relatively consistent within all samples, the signal of both RuO_3H and RuO_2Cl fragments significantly decreased with surface area (Figure 4C,D), and they were the highest for Ru/TiO_2-R and the lowest for Ru/TiO_2-S, Ru/TiO_2-T, and Ru/TiO_2-B samples. This indicated the formation of different Ru species and the different local environments of Ru in the as-prepared catalysts.

The XPS spectrum of the Ru-TiO_2 catalysts contained Ru 3d and Ru 3p bands as two main features, which, in this case, overlapped with C 1s and Ti 2p bands, respectively, as reported previously.[29] Figure S5 depicts that the strong contribution of Ti 2p from the TiO_2 support made Ru 3p undetectable in most cases. Therefore, the analysis was focused on another region, where Ru 3d features with a doublet separation of 4.17 eV[30] could be clearly distinguished from characteristic C−C, C−O, and C═O species from adventitious carbon[31] (Figure 5A). XPS analysis of the dried catalysts was in line with TOF-SIMS analysis and confirmed the presence of Ru−OH species, indicating that $RuCl_3$ underwent hydrolysis during the synthesis of Ru/TiO_2 catalysts. The Ru $3d_{5/2}$ spectrum was dominated by peaks with the binding energies of 280.7 and 282.3 eV, attributed to surface Ru−OH and Ru−O species, respectively.[30] The intensity of these peaks was comparable in the spectra of all samples except that of 1Ru/TiO_2-R, where the contribution of the Ru−O species was negligible. In this case, a third signal at 282.9 eV assigned to Ru−Cl[30] was also observed in addition to the predominant Ru−OH peak. This indicated the incomplete hydrolysis of $RuCl_3$ in this sample or the formation of a mixed species. Conversely, the Ru−Cl signal was absent in the spectra of other samples, albeit it was also barely noticeable in 1Ru/TiO_2-A. These species differed from the formal RuO_2Cl species detected by TOF-SIMS, which is expected to appear at 281.3 eV.[32] This indicated that Cl was retained on the titania surface but not in close contact with Ru. The use of the more top-surface-sensitive TOF-SIMS technique confirmed the very limited interaction between Ru and Cl, as evidenced by only a

https://doi.org/10.1021/acssuschemeng.5c04908
ACS Sustainable Chem. Eng. 2025, 13, 11652−11667

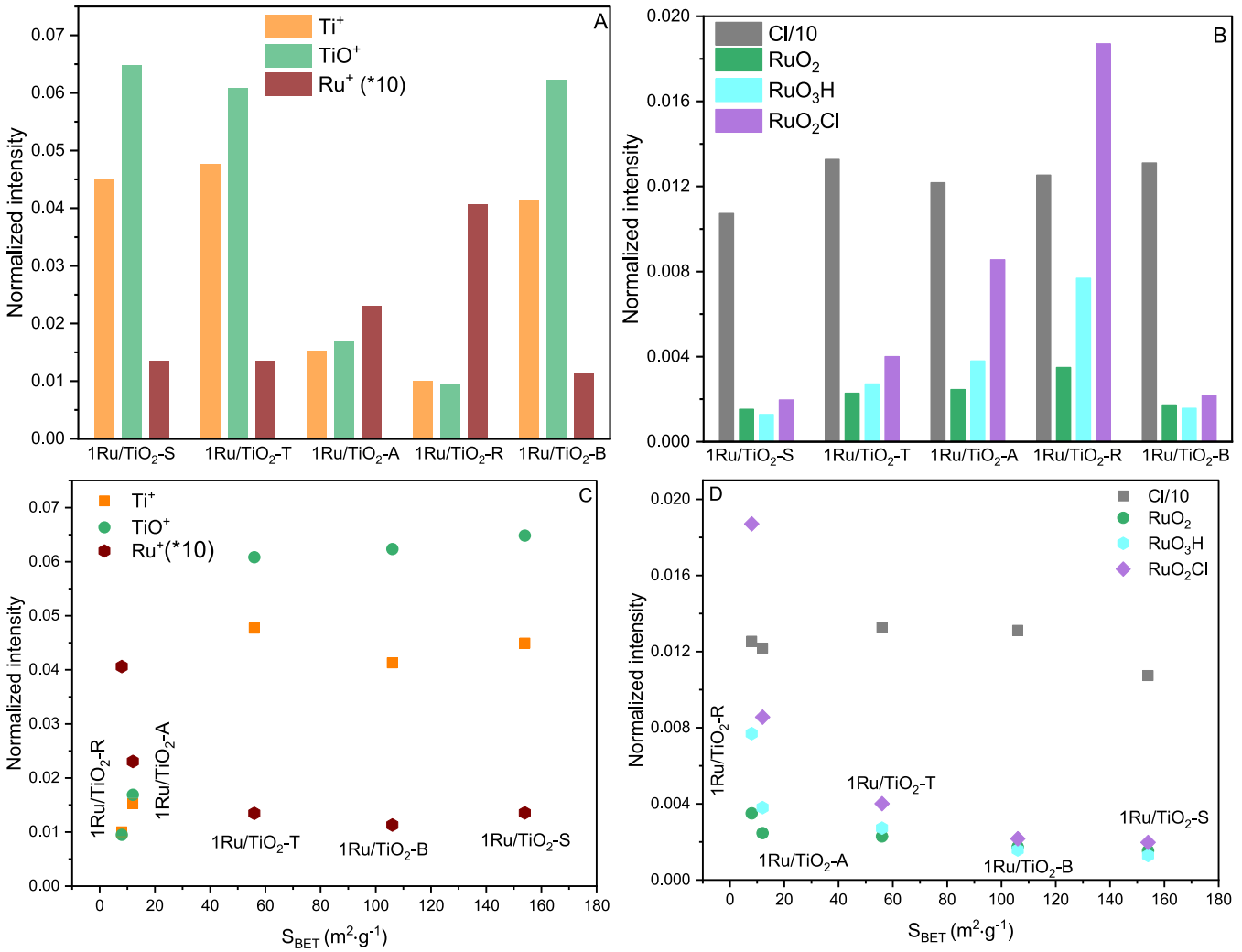

Figure 4. TOF-SIMS analysis: positive spectra (A), negative spectra (B). The dependence of signal intensity on the SBET of Ru/loaded catalysts (C, D).

very weak signal of RuO_2Cl^- ions. Instead, in the high surface area samples, Ru was mainly present as Ru−O or Ru−OH species on the surface of titania. Therefore, we could assume that in this case, the TiO_2 surface was enriched with the combination of phases close to $RuCl(OH)_2$ and $Ru(OH)_3$.

Given the evidence for residual Cl species by XRF and their potential impact on the activity,[33] the Cl 2p region was analyzed as well (Figure 5B). While surface Cl was detected in all samples, it was not exclusively bound to Ru in all cases. The Cl 2p doublet, with $2p_{3/2}$ at 198.2 eV, was more consistent with hydrolysis products of $RuCl_3$.[30] Nonetheless, only $1Ru/TiO_2$-R showed higher intensity and contribution from Ru−Cl species, with the $2p_{3/2}$ peak at 199.6 eV.[30] This confirms the presence of Cl-bound Ru in the Ru 3d spectrum of this sample, whereas in other samples, Cl was mainly bound to the TiO_2 surface, separate from Ru.

The quantification of overall Ru and Cl surface content relative to Ti surface content was evaluated based on the intensity of Ru 3d, Ti 2p, and Cl 2p peaks (Figure S6). In contrast to the XRF results, surface quantification revealed significantly lower Cl content relative to Ru. Comparing all samples, both surface Ru/Ti and Cl/Ti ratios followed the same trend, inversely proportional to the surface area (Figure S6).

The Ru−−titania interaction and the reducibility of Ru/TiO_2 catalysts were studied by H_2-TPR. First, the pristine TiO_2 supports were investigated (Figure S7). The reduction profiles showed a peak at >400 °C, which could be attributed to the reduction of the titania subsurface (indicated also by a typical change in color),[34,35] while the reduction of bulky TiO_2 typically occurred at >800 °C.[34] The intensity of the surface reduction peak increased with increasing TiO_2 surface area. The TPR profiles of Ru catalysts (Figure 6) showed additional peaks at temperatures lower than 470 °C associated with the presence of Ru nanoparticles and surface modifications induced by Ru. These profiles generally revealed two sets of peaks, in the range of 70−200 °C (low temperature, LT) and 250−500 °C (high temperature, HT), respectively. According to the previous literature, both peaks corresponded to the different interactions of Ru nanoparticles with titania, and their position was influenced by the Ru size and Ru particle size distribution.[36,37]

The first LT peak at about 150 °C represented the reduction of small and loosely bonded Ru^{3+} nanoparticles.[38,39] The peak intensity was more expressed as the surface area decreased. The peak at 201 °C observed only for the $1Ru/TiO_2$-A sample corresponded to the reduction of weakly supported RuO_2 species.[39] The HT peak observed in the range of 250−450 °C was associated with the reduction of Ru/TiO_2 interphase sites,

https://doi.org/10.1021/acssuschemeng.5c04908
ACS Sustainable Chem. Eng. 2025, 13, 11652−11667

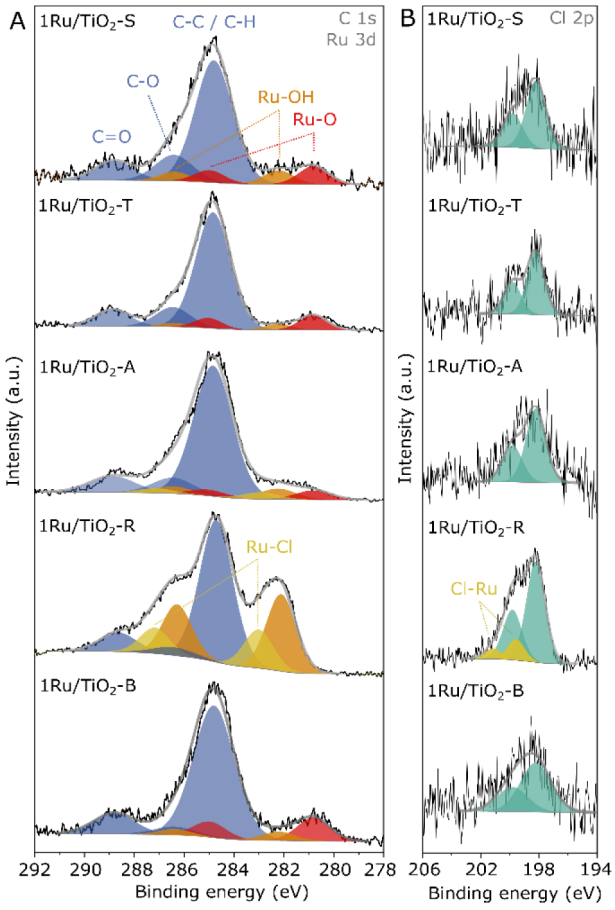

Figure 5. High-resolution XPS spectra of C 1s and Ru 3d regions (A) and Cl 2p region (B) for 1Ru/TiO_2 catalysts.

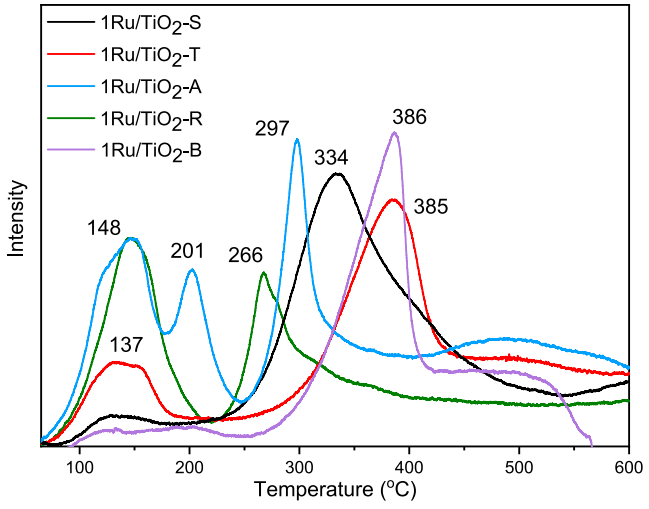

Figure 6. Temperature-programmed reduction profiles of 1Ru/TiO_2 catalysts.

which resulted from the strong Ru−TiO_2 interaction facilitating the reduction of the titania surface.[40−43] The area of this peak roughly correlated with the TiO_2 surface area. The facilitated reduction of titania surface was attributed to a hydrogen spillover, i.e., a phenomenon typical for metal-based catalysts.[34,44]

The catalyst degree of reducibility was calculated using eq 4. The observed H_2 consumption was 1.5−2 times higher than the theoretical values (calculated for Ru^{3+} to Ru^0 reduction, Table S1). The increased H_2 consumption could be explained either by partial reduction of the titania surface as discussed above or by a hydrogen spillover.[34]

3.3. Study of Reduced Ru Catalysts. Reduced Ru/TiO_2 catalysts were characterized to describe the transformation of Ru species on the catalyst surface under hydrogenation conditions. The residual Cl content after *ex situ* reduction at 400 °C was determined by XRF. In comparison with as-prepared catalysts, the Cl content significantly decreased, although its residual content was still between 0.03 and 0.70 wt % (Table 3). After the reduction step, Cl content in the samples decreased by 27, 43, 61, 84, and 90% for 1Ru/TiO_2-S, 1Ru/TiO_2-B, 1Ru/TiO_2-T, 1Ru/TiO_2-A, and 1Ru/TiO_2-R, respectively. This strongly indicated that Cl bound to Ru species was removed, while chlorine on the titania surface was not removed during the reduction treatment.

Ru dispersion and particle size were assessed using HR-STEM (Figures 7 and 8). HR-STEM revealed that the size of Ru particles was in the range of 1−2 nm for most catalysts, except for 1Ru/TiO_2-R where particles with a mean particle diameter of 3.4 nm were observed (Figure 7). The values of Ru particle size calculated based on STEM analysis decreased with increasing S_{BET} (Figure 9A). STEM images (here exemplified by 1Ru/TiO_2-A, Figure 8) revealed the only presence of hexagonal (hcp) Ru nanoparticles in all of the prepared samples. The hcp particles exhibited typical *d*-spacings of 2.05 Å and 2.14 Å for Ru (101) and Ru (002), respectively.

The specific surface area of Ru was calculated based on the determined size and hcp shape of Ru particles (Table 3). The calculated Ru specific surface area was in the range of 0.9−3.1 $m^2 \cdot g^{-1}$, the highest in case of 1Ru/TiO_2-S. Comparing the Ru specific surface area and TiO_2 surface area (Table 2), the support surface area was almost 50 times larger in case of 1Ru/TiO_2-S, while it was only about 10 times larger in case of 1Ru/TiO_2-A and 1Ru/TiO_2-R. This contributed to the observed larger intensity of Ti ions compared to Ru ions in the latter two samples in TOF-SIMS analysis (Figure 4).

FTIR-CO with *in situ* reduction was used to describe the charge of Ru particles in reduced catalysts.[45] The FTIR spectra of adsorbed CO (Figure 10) revealed the existence of numerous bands at 2135, 2110, 2070, 2050, 2025, and 2000 cm^{-1}. Generally, bands below 2050 cm^{-1} are attributed to CO adsorption on Ru^0 particles, whereas bands at higher wavenumbers correspond to multicarbonyl species attached to partially oxidized Ru^{n+} sites on the interface.[46] The higher the partial charge of Ru, the weaker the interaction between CO and the metal, resulting in higher wavenumber bands for the adsorbed CO. The spectrum of 1Ru/TiO_2-S-red evidenced the presence of the most intense bands at 2040 cm^{-1} associated with the linear CO adsorption on Ru^0[47] and the bands at 2000 and 1980 cm^{-1} characteristic of the top adsorbed CO species at different sites of metallic Ru nanoparticles, whereas the least intense bands at 2000 cm^{-1} appeared in the spectrum of 1Ru/TiO_2-R-red (Figure 10). This demonstrates that 1Ru/TiO_2-S-red had the most accessible surface metallic Ru sites, while 1Ru/TiO_2-R-red had the lowest number of reduced Ru sites, which correlated with the Ru dispersion and Ru-specific surface area evaluated from TEM (Table 3). For other catalysts, the wavenumbers of the primary CO bands indicated the predominance of partially charged Ru species over metallic Ru^0. It is worth noting that Ru^0 could be partially oxidized by CO via a reaction of surficial −OH, CO, and Ru^0, which is not

https://doi.org/10.1021/acssuschemeng.5c04908
ACS Sustainable Chem. Eng. 2025, 13, 11652−11667

Table 3. Characterization Data of Reduced Catalysts

Material	w_{Ru} (wt %)	w_{Cl} (wt %)	n_{Ru}/nm^2 density	n_{Cl}/n_{Ru} bulk	d_{Ru} (nm)[a]	D_{Ru} (%)[b]	S_{Ru} ($m^2 \cdot g^{-1}$)[c]
1Ru/TiO_2-S-red	0.83	0.73	0.4	2.5	1.0	81	3.1
1Ru/TiO_2-T-red	0.94	0.32	1.0	1.0	1.6	50	1.9
1Ru/TiO_2-A-red	0.89	0.08	4.6	0.3	2.0	40	1.5
1Ru/TiO_2-R-red	0.90	0.03	7.2	0.1	3.4	24	0.9
1Ru/TiO_2-B-red	0.81	0.63	0.5	2.2	1.2	67	2.5

[a]Determined by TEM. [b]Calculated using eq 5. [c]Calculated using eq 6.

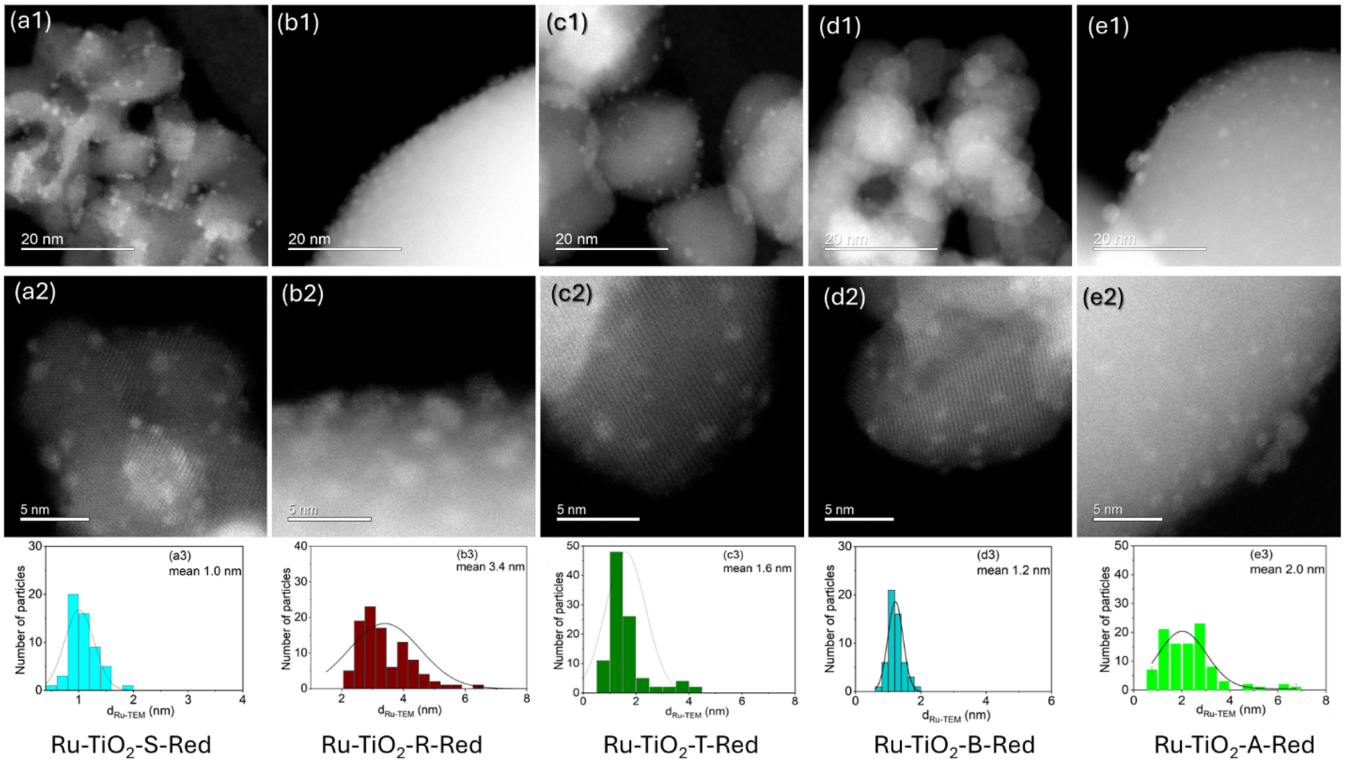

Figure 7. Morphology and particle size distributions of (a) Ru-TiO_2-S-red, (b) Ru-TiO_2-R-red, (c) Ru-TiO_2-T-red, (d) Ru-TiO_2-B-red, and (e) Ru-TiO_2-A-red.

possible to avoid.[45] The band intensities correlated with the size of the Ru particles and surface area. TiO_2 supports with a larger surface area facilitated the formation of smaller and properly reduced Ru nanoparticles, providing greater availability of adsorption sites on the metal surface.

The effect of a reduction step on the state of the surface was assessed by XPS with the *ex situ* reduction of Ru/TiO_2 samples at 400 °C. Figure 11A shows that the H_2 treatment caused significant changes in the Ru 3d spectrum, where a doublet $3d_{5/2}$ at 279.7 eV, characteristic for metallic Ru^0,[30] was the dominant feature. Despite the fact that the Ru particle size and dispersion were influenced by the various titania (Table 3), this did not dramatically affect the oxidation state of surface Ru. In the studied samples, the XPS spectra showed consistent features of Ru−OH and Ru−O species, albeit at lower intensities.

The absence of Ru−Cl species in catalysts with a lower surface area was confirmed by the disappearance of Cl peaks in the Cl 2p region (Figure 11B). Among the samples, 1Ru/TiO_2-S-red retained the highest Cl content, while Cl 2p signals were extremely low or absent in the spectra of other samples. This might occur due to the applied vacuum prior to XPS and the more efficient Cl release. Despite the significant reduction in Cl content for most samples, the H_2 pretreatment had minimal impact on the Ru/Ti atomic ratio at the surface, as illustrated in Figure S8. This suggests that the reduction step did not significantly affect the distribution of Ru on the catalyst surface.

3.4. Catalyst Performance and Selectivity in HMF Conversion. The performance of all prepared Ru catalysts was evaluated in HMF conversion at 220 °C and 70 bar of H_2 (Figure 12A). Under the used reaction conditions, HMF conversion over Ru/TiO_2 catalysts was >90% after 3 h in all cases. The initial catalyst activity at 5 min was monitored as a function of surface area (Figure 12B), Ru particle size (Figure 12C), Ru specific surface area (Figure 12D), Cl/Ru (Figure 12E), and propene peak area (m/z 41) obtained in IPA-TPD experiments (Figure 12F). It can be observed that 1Ru/TiO_2-B and 1Ru/TiO_2-S, having both a larger support surface and larger Ru specific surface area due to smaller Ru particles, had higher initial activity. Besides Ru particle size, the acidity of the supports also plays a crucial role in catalytic activity. It has been reported that the anatase phase was richer in Lewis acid sites compared to rutile phase,[48] which could enhance HMF adsorption and, in turn, its conversion, or even provide intrinsic catalytic activity. In fact, we have reported the intrinsic catalytic activity of neat TiO_2 supports in HMF conversion due to Lewis acid sites.[13] This is corroborated by the increasing initial HMF

https://doi.org/10.1021/acssuschemeng.5c04908
ACS Sustainable Chem. Eng. 2025, 13, 11652−11667

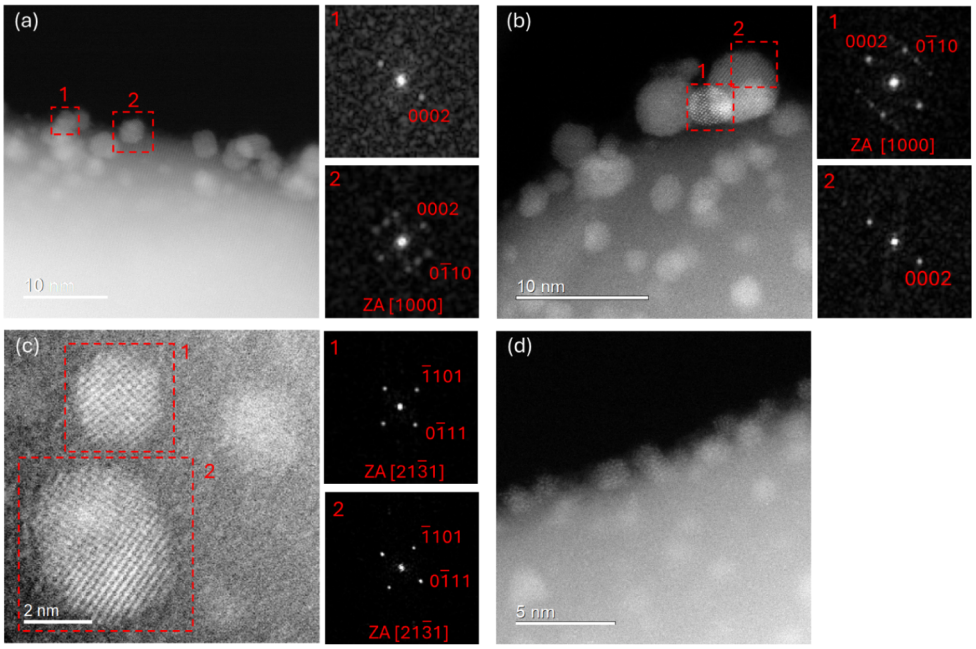

Figure 8. STEM-ADF images of 1Ru/TiO_2-A-red showing the hcp structure of Ru particles: (a) nanoparticles with different sizes located on the surface of the TiO_2-A support, (b) the closer location of larger particles with different orientations, (c) two nanoparticles oriented with a particular zone axis [21$\bar{3}$1] on the TiO_2-A support, and (d) smaller 1−2 nm Ru nanoparticles on the surface of the TiO_2-A support.

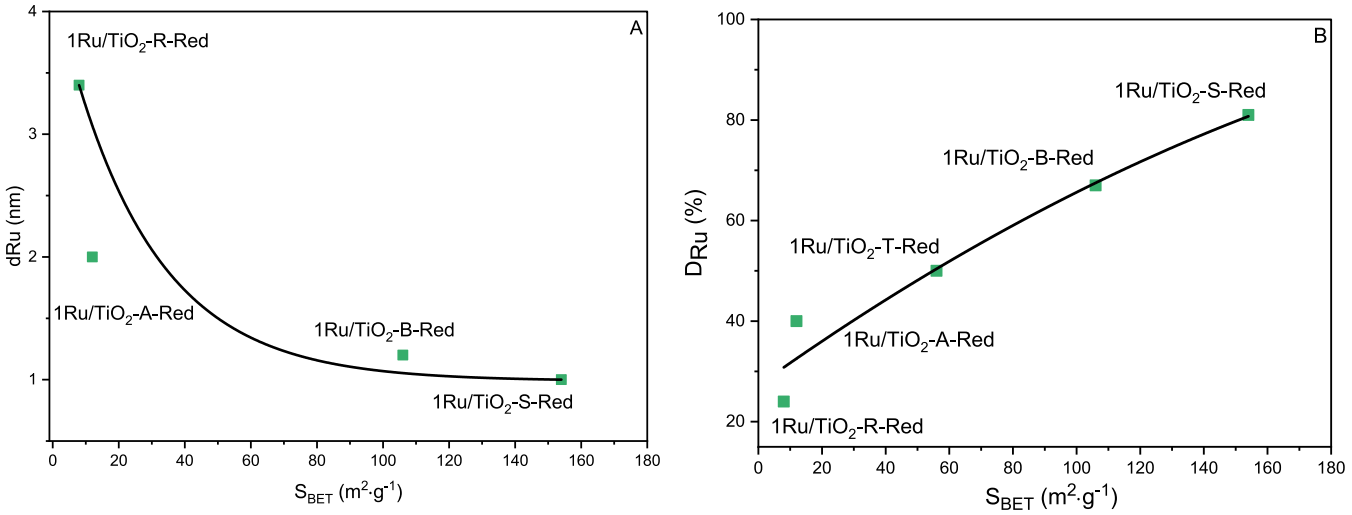

Figure 9. Dependence of Ru particle size determined from TEM on the catalyst surface area (A) and Ru dispersion (B).

activity with increasing propene peak areas obtained in IPA-TPD experiments (Figure 12F). In other words, the larger the number of acid sites, the higher the initial rate of HMF conversion. Additionally, the concentration of S in the used HMF was analyzed since S could be a catalyst poison influencing the conversion.[49] The measured negligible content of S < 1 mg/kg indicated that HMF did not contain any S-containing compounds and that catalyst poisoning by sulfur could be excluded.

HMF can undergo numerous reactions on oxide-supported metals. On the metal sites, hydrogenation and hydrogenolysis are the main reactions in the presence of H_2. On TiO_2 support, HMF is primarily adsorbed and activated prior to these reactions, but it can also undergo disproportionation that occurs even in the absence of H_2.[13]

Figure 13 depicts the distribution of the main reaction products formed over different Ru/TiO_2 catalysts, while Figure S9 presents the yield of other minor products. 5-MF was the main reaction product formed over 1Ru/TiO_2-S, 1Ru/TiO_2-T and 1Ru/TiO_2-B. This product can be formed either by a disproportionation mechanism on the acid Lewis sites of TiO_2[13] or by the direct hydrogenolysis of HMF over small Ru particles (pathways A and B in Scheme 1, Figure 13A), which aligns with the reported literature.[16] Previously, we reported that the disproportionation of HMF over metal-free TiO_2 produces almost equimolar amounts of 2,5-diformylfuran (2,5-DFF) and 5-methylfurfural (5-MF) (pathway A in Scheme 1).[13] Nevertheless, 2,5-DFF was not detected among the reaction products formed over all Ru/TiO_2 catalysts studied. Presumably, this dialdehyde was quickly rehydrogenated back to HMF. Besides the hydrogenolysis/disproportionation steps, HMF was directly

https://doi.org/10.1021/acssuschemeng.5c04908
ACS Sustainable Chem. Eng. 2025, 13, 11652−11667

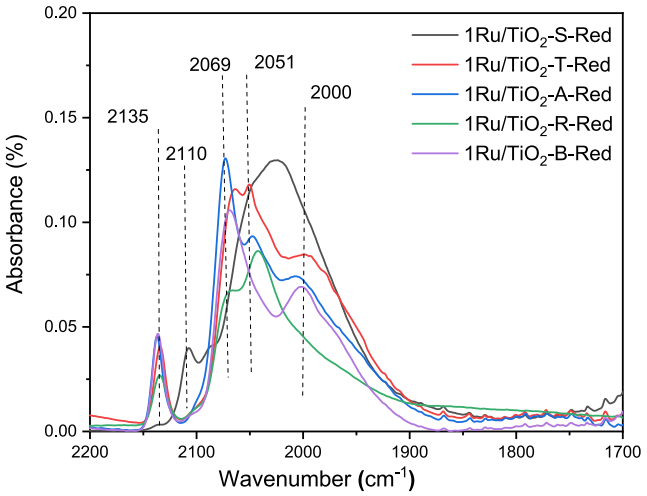

Figure 10. Comparison of CO adsorption on reduced 1Ru/TiO_2-red catalysts.

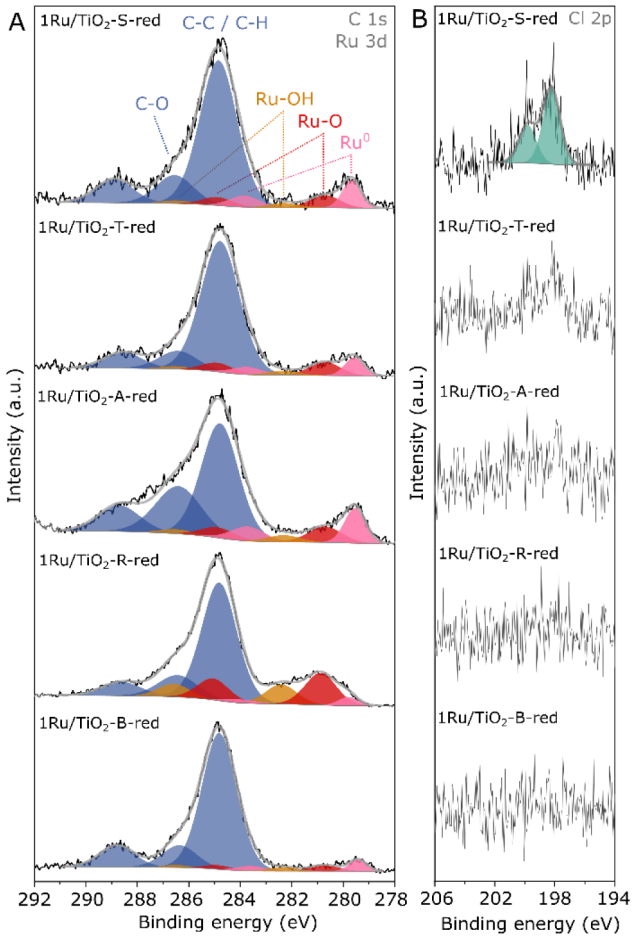

Figure 11. High-resolution XPS spectra of the C 1s/Ru 3d (A) and Cl 2p (B) regions from 1Ru/TiO_2-red samples treated with H_2 at 400 °C.

hydrogenated over Ru active sites to produce 2,5-bis-(hydroxymethyl)furan (BHMF) as a key hydrogenated product (pathway C in Scheme 1). Apart from others, 1Ru/TiO_2-R and 1Ru/TiO_2-A with the lowest surface area exhibited different catalytic performance. The yield of BHMF was negligible over 1Ru/TiO_2-S, 1Ru/TiO_2-T, and 1Ru/TiO_2-B catalysts, while 1Ru/TiO_2-A and 1Ru/TiO_2-R were more selective toward BHMF, with the yields of 34 and 52%, respectively. Moreover, BHMF was further hydrogenolyzed to 5-MFA over 1Ru/TiO_2-A with a yield of 30% and over 1Ru/TiO_2-R with a yield of 14%, followed by the formation of DMF.

This could be the consequence of two phenomena:

i) The higher number of Lewis acid sites on TiO_2-S, TiO_2-B, and TiO_2-T surfaces contributed to the disproportionation or hydrogenolysis routes and therefore the formation of 5-MF prevailed. As observed in our previous investigation,[13] TiO_2 supports with a higher surface area exhibited enhanced Lewis acidity, which facilitated the adsorption of HMF through its hydroxyl functionality. Thus, a linear correlation between the formation of 5-MF against surface area and the propene peak was observed (Figures 14B, E). The role of acid sites in HMF hydrogenolysis was also observed in HMF conversion to DMF with 5-MF as the main reaction intermediate.[50,51]

ii) The difference in hydrogenolysis activity of smaller (1.0 nm) and larger (3.4 nm) Ru particles. Due to the concurrent effect of Ru and the support on the activity, it was difficult to discern a clear influence of the size of Ru particles on the course of the reaction. Nonetheless, the reaction over 1Ru/TiO_2-T (1.6 nm) and 1Ru/TiO_2-A (2.0 nm) showed a switchable formation of 5-MF or BHMF, respectively, as the main product. Moreover, there was a difference between both low-surface area samples 1Ru/TiO_2-A (2.0 nm) and 1Ru/TiO_2-R (3.4 nm) as the successive hydrogenation of BHMF to BHTHMF was observed over 1Ru/TiO_2-R, while this consecutive hydrogenation product was not observed over 1Ru/TiO_2-A at all (see Figure 13). The trendlines of 5-MF and BHMF yields presented in Figure 14 clearly demonstrate their opposite dependence on the key catalyst parameters, such as specific surface area, surface properties, and Ru particle size.

Several studies showed that larger Ru particles are beneficial for the C═O group hydrogenation rather than for ring hydrogenation. Galvagno et al. reported that the adsorption of an aromatic group in cinnamaldehyde became difficult with the increase in Ru particle size in Ru/C; consequently, the C═O bond was positioned closer to the catalyst surface than the C═C bond.[52] This was consistent with the previous study of Newman et al., who found that phenol hydrogenolysis was facilitated by smaller Ru particles.[53] Despite the fact that those studies revealed the effect of Ru particle size, our data evidence that the support properties determine the catalyst behavior to a large extent. As HMF conversion increased, the yield of both key products decreased due to the subsequent hydrogenolysis/hydrogenation of BHMF to 5-MFA (Figure 13B) and 5-methyl tetrahydrofurfuryl alcohol (5-MTHFA, Figure 13E), while BHMTHF, a product of BHMF hydrogenation, was found only over 1Ru/TiO_2-R catalyst (Figure 13D).

The total mass balance was considered as a function of HMF conversion (Figure S10). After 3 h, the mass balance fluctuated between 75 and 95% depending on the catalyst's specific surface area. As the surface area was higher, the mass balance decreased; this could be due to the side reactions happening on the surface with more acidic sites, for example, 1Ru/TiO_2-S. The simple stability test in a flow reactor was performed and is described in Figure S13.

https://doi.org/10.1021/acssuschemeng.5c04908
ACS Sustainable Chem. Eng. 2025, 13, 11652−11667

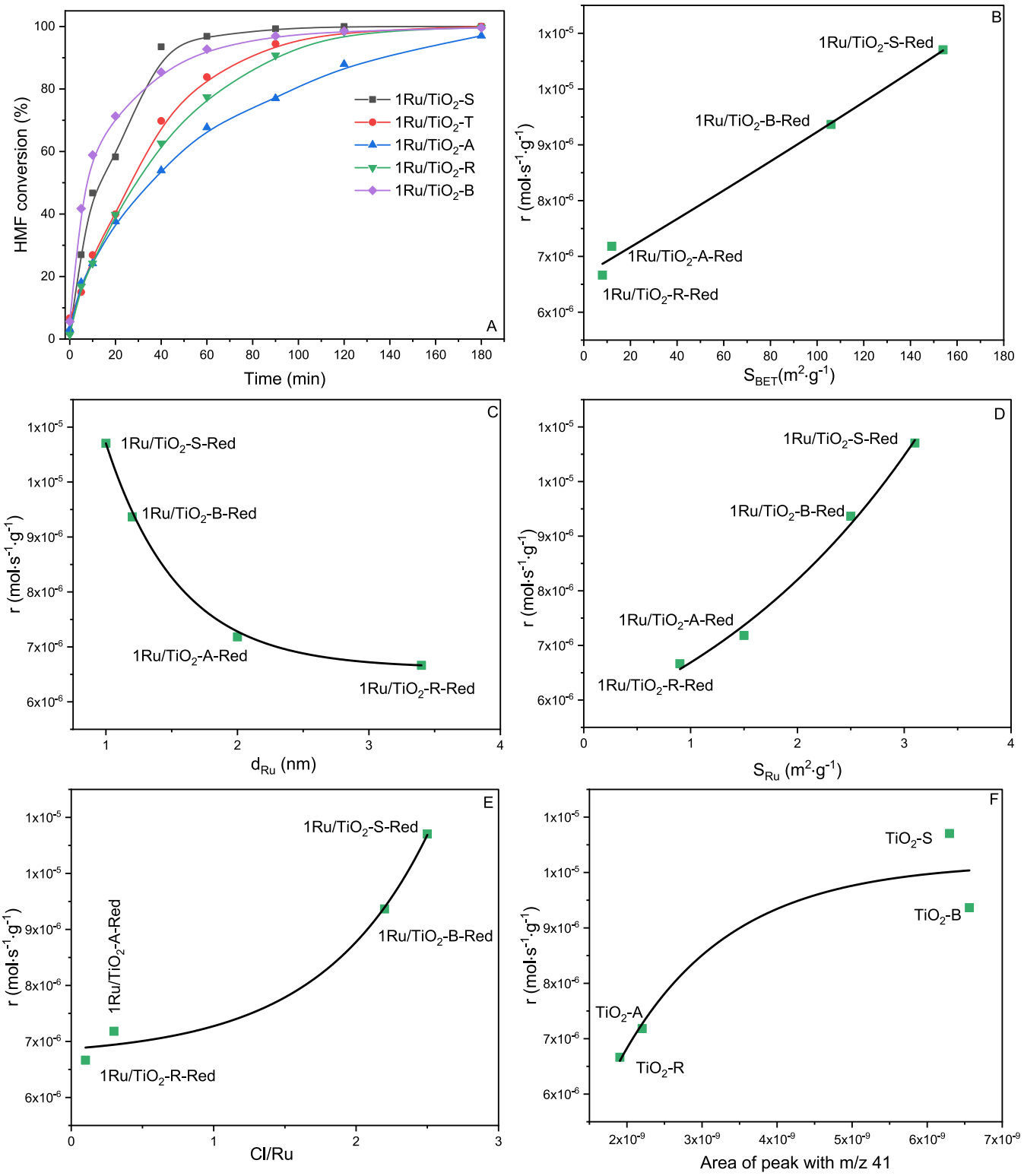

Figure 12. Change in HMF conversion with reaction time (A). The initial rate of reaction at 5 min as a function of surface area (B), Ru particle size (C), Ru specific surface area (D), bulk Cl/Ru ratio (E), and propene peak area ($m/z = 41$) obtained in IPA-TPD (F). The lines shown merely represent the trend of the data and do not involve any data fitting.

3.5. Analysis of Spent Catalysts. Elemental organic analysis was used to determine the carbon content in the spent catalysts. The carbon content in the spent samples varied from 1.1 to 19.8 wt % in dependence on the surface area of Ru/TiO_2 catalysts (Table 4). The carbon content was normalized by the surface area (eq 7) of the corresponding 1Ru/TiO_2 catalysts (Table 4, SA_C) to evaluate the carbon density on the surface.

To understand the nature of carbon species, 1Ru/TiO_2-S-spent, 1Ru/TiO_2-A-spent, and 1Ru/TiO_2-R-spent samples were calcined at 200 and 400 °C, and the change in surface carbon was tracked using ELOA (Table S2). The treatment at 200 and 400

https://doi.org/10.1021/acssuschemeng.5c04908
ACS Sustainable Chem. Eng. 2025, 13, 11652−11667

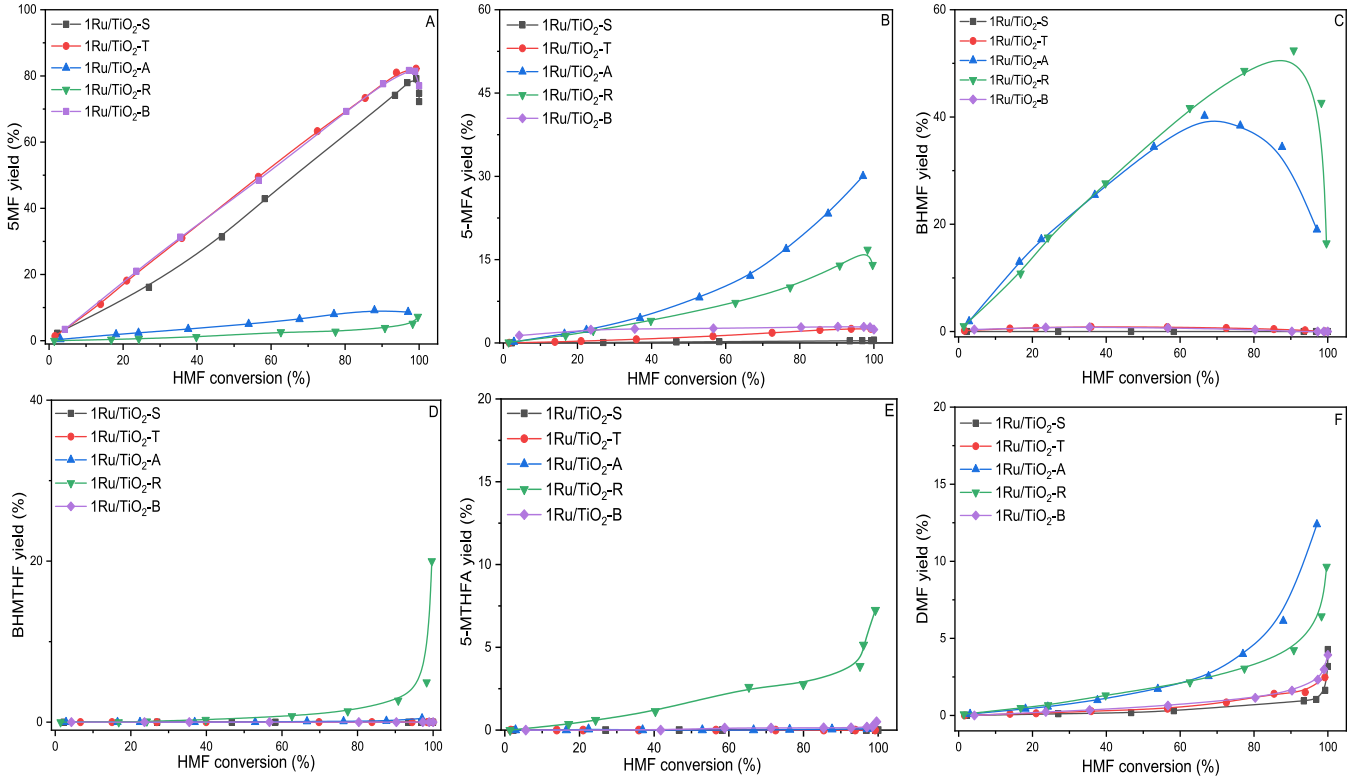

Figure 13. Product yields as a function of HMF conversion over 1Ru/TiO_2-X at 220 °C and 70 bar H_2 in THF. Figures A–F correspond to (A) 5-methylfurfural (5-MF), (B) 5-methylfurfuryl alcohol (5MFA), (C) 2,5-bis(hydroxymethyl)furan (BHMF), (D) 2,5-bis(hydroxymethyl)-tetrahydrofuran (BHMTHF), (E) 5-methyl-2-tetrahydrofurfurylalcohol (5-MTHFA), and (F) 2,5-dimethylfuran (DMF), respectively.

Scheme 1. Proposed Reaction Pathways of HMF Conversion over Ru/TiO_2 Catalysts

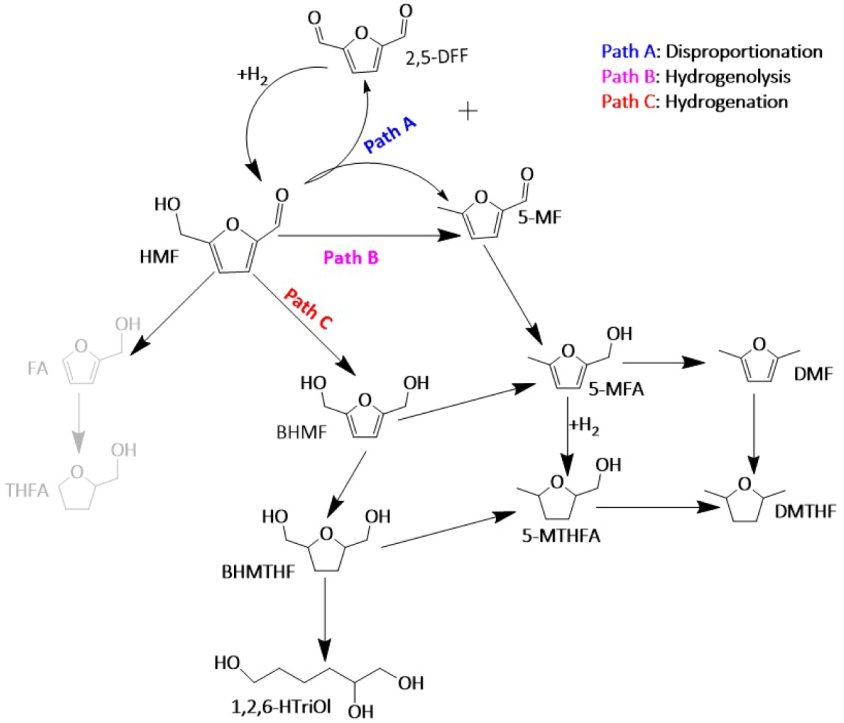

°C resulted in the almost complete removal of carbon from the materials, and the C/H molar ratio indicated the presence of aromatic and polyaromatic compounds over the surface of the catalyst, which reflected the aromatic nature of HMF molecules. The C/H ratio could, however, bear some error, as the contribution of H originating from the titania support (titanyl groups) cannot be excluded. According to TGA-MS, the mass loss of 26 wt % occurred between 200 and 400 °C (Figure S11).

https://doi.org/10.1021/acssuschemeng.5c04908
ACS Sustainable Chem. Eng. 2025, 13, 11652−11667

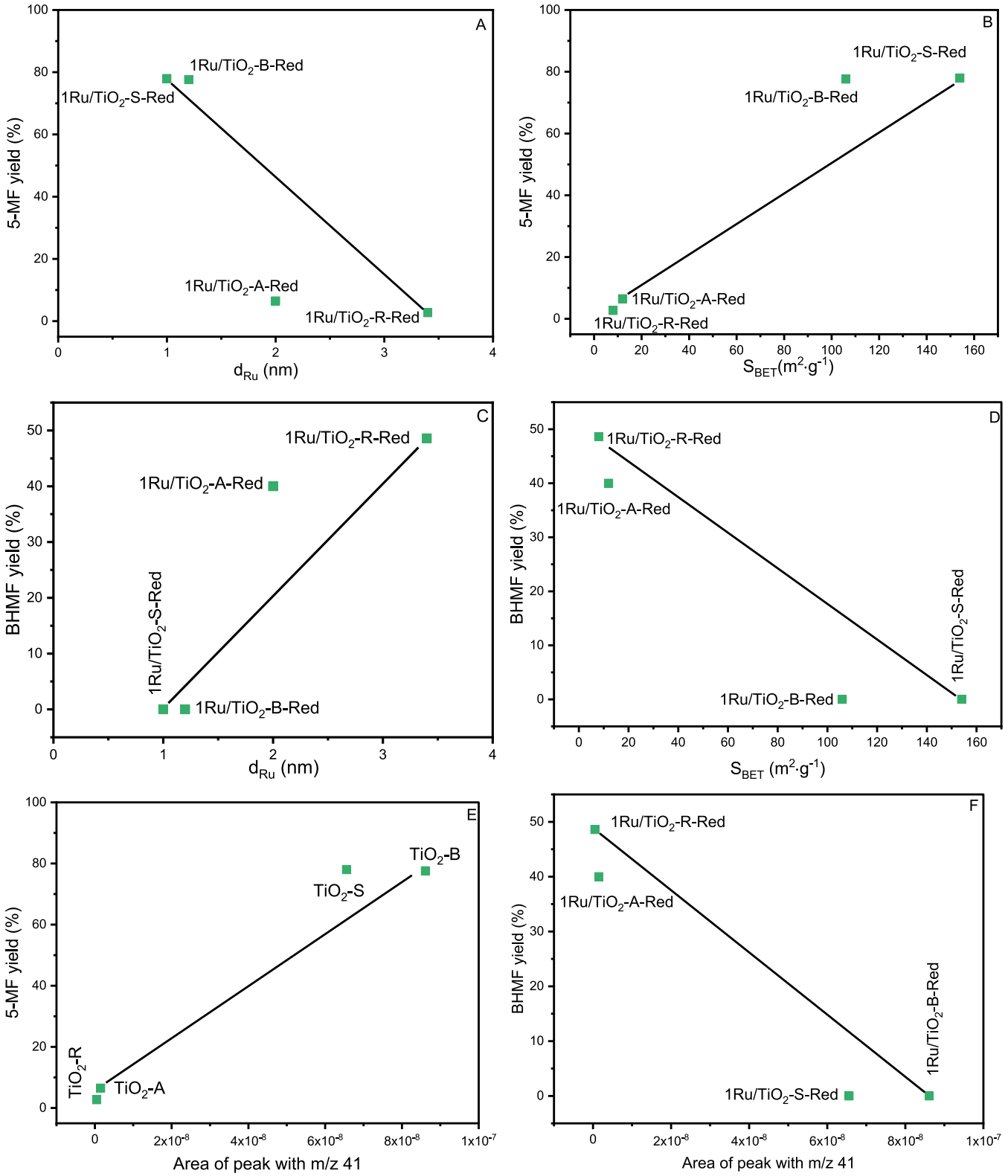

Figure 14. Dependence of (A) 5-MF yield at 90% HMF conversion on the Ru particle size, (B) 5-MF yield on the surface area Ru/TiO_2, (C) BHMF yield on the Ru particle size, (D) BHMF yield on the surface area Ru/TiO_2, (E) 5-MF yield on the propene peak area (m/z 41), and (F) BHMF yield on the propene peak area (m/z 41). The shown lines merely represent the trend of the data and do not involve any data fitting.

In this step, mostly CO_2 and H_2O were released, which indicated the presence of adsorbed organics or fragments of moieties from oxygenates. The literature suggests that within that temperature range, a coke with oxygenated bonds is being burned,[54] implying that the observed mass loss may be due to the decomposition of adsorbed oxygenates. The presence of oxygenates was indicated by DRIFT analysis (not presented data), where specific bands for C−O, C═O, and −OH groups were detected. Previous studies declared that furfural species have a strong adsorption ability on metal-supported catalysts, causing catalyst deactiva-

https://doi.org/10.1021/acssuschemeng.5c04908
ACS Sustainable Chem. Eng. 2025, 13, 11652−11667

Table 4. Elemental Organics Analysis and Particle Size of Spent Catalysts (after 3 h Experiment at 220 °C and 70 Bar H_2)

Sample	w_C (wt %)	SA_C (at/nm^2)	w_H (wt %)	C/H mol/mol	d_{TiO2} (nm)
1Ru/TiO_2-S-spent	19.8	65	1.9	0.9	17[a]
1Ru/TiO_2-T-spent	12.6	113	1.2	0.8	25[a]
1Ru/TiO_2-A-spent	5.4	226	0.5	1.1	126[a]
1Ru/TiO_2-R-spent	1.1	69	0.1	0.9	316[b]
1Ru/TiO_2-B-spent	14.3	68	1.4	0.8	13[a]

[a]Anatase. [b]Rutile, wc is the determined carbon content, SAc is the molar amount of C normalized per surface area, wH is the determined H content, and C/H is the molar ratio of determined C and H.

tion.[55] Spent samples were analyzed to assess their morphological changes by XRD. TiO_2 mean crystallite size in spent catalysts showed negligible changes (Table 1). However, further evaluation of XRD patterns (Figure S12) revealed a new reflection at $2\theta = 26.5°$, which was attributed to graphitic carbon (JCPDS 01-086-8296).

4. CONCLUSIONS

TiO_2 is widely used as a support for Ru-based catalysts, which can be employed in HMF valorization. However, the influence of its surface properties on the formation of Ru active species in Ru/TiO_2 catalysts and catalytic performance has rarely been addressed. To address this gap, we considered using five different TiO_2 supports varying in their surface and phase composition to load 1 wt % of Ru using $RuCl_3$. Generally, the inherent properties of titania strongly affected the final characteristics of Ru active sites: their structure, local environment, and activity.

The use of a TiO_2 support with a larger BET surface area and higher number of Lewis acid sites promoted the formation of smaller Ru particles (1.0−1.6 nm) with greater Ru dispersion (50−81%). This enhanced the availability of Ru sites, whose local environment was characterized by the formation of surface Ru−O species. On the other hand, employing TiO_2 support with a lower surface area and fewer acid sites resulted in the formation of larger Ru particles (2.0 and 3.4 nm). In this case, the local environment of Ru changed, rather exhibiting Ru−Cl species on the titania surface. All these characteristics strongly influenced the activity and selectivity of Ru/TiO_2 catalysts in HMF hydrogenation.

The catalytic performance of the studied Ru/TiO_2 catalysts in HMF hydrogenation significantly varied. The catalysts formed from high-surface-area TiO_2 with smaller Ru particles showed enhanced performance in HMF conversion due to a larger number of Lewis sites and yielded primary 5-MF. On the other hand, small-surface-area TiO_2 bearing larger Ru particles switched the catalyst selectivity toward BHMF. This highlights the essential role of titania and reflects the role of Ru particle size, where the small Ru particles apparently are not active in hydrogenation.

This study highlights the critical role of the surface properties of the titania support in the formation of Ru catalysts. These findings provide valuable insights for optimizing Ru/TiO_2 catalysts in applications where factors like Ru dispersion, oxidation state, and interaction with support strength as well as the acidity of pure supports are key determinants of catalytic performance.

■ ASSOCIATED CONTENT

Supporting Information

The Supporting Information is available free of charge at https://pubs.acs.org/doi/10.1021/acssuschemeng.5c04908.

Additional XRD, TPR, and TGA patterns; TEM images; FTIR and XPS spectra; yields of minor side products; H_2-uptake and ELOA analysis data (PDF)

■ AUTHOR INFORMATION

Corresponding Author

Jaroslav Aubrecht − *Department of Sustainable Fuels and Green Chemistry, University of Chemistry and Technology, Prague 6 166 28, Czech Republic;* orcid.org/0000-0002-2730-7040; Email: aubrechj@vscht.cz

Authors

Babar Amin − *Department of Sustainable Fuels and Green Chemistry, University of Chemistry and Technology, Prague 6 166 28, Czech Republic*

Oleg Kikhtyanin − *Technopark Kralupy, Kralupy nad Vltavou 278 01, Czech Republic*

Evgeniya Grechman − *Department of Sustainable Fuels and Green Chemistry, University of Chemistry and Technology, Prague 6 166 28, Czech Republic*

Gustavo Andrade Silva Alves − *Institute of Materials Chemistry, Technische Universität Wien, Vienna 1060, Austria*

Alberto Tampieri − *Institute of Materials Chemistry, Technische Universität Wien, Vienna 1060, Austria*

Karin Föttinger − *Institute of Materials Chemistry, Technische Universität Wien, Vienna 1060, Austria;* orcid.org/0000-0002-2193-0755

Marcin Jędrzejczyk − *Institute of General and Ecological Chemistry, Lodz University of Technology, Łódź 90-924, Poland;* orcid.org/0000-0003-2795-5782

Agnieszka M. Ruppert − *Institute of General and Ecological Chemistry, Lodz University of Technology, Łódź 90-924, Poland;* orcid.org/0000-0001-5704-2461

Francisco Ruiz-Zepeda − *Department of Materials Chemistry, National Institute of Chemistry, Ljubljana SI-1000, Slovenia*

David Kubička − *Department of Sustainable Fuels and Green Chemistry, University of Chemistry and Technology, Prague 6 166 28, Czech Republic; Technopark Kralupy, Kralupy nad Vltavou 278 01, Czech Republic;* orcid.org/0000-0003-2996-7824

Complete contact information is available at: https://pubs.acs.org/10.1021/acssuschemeng.5c04908

Author Contributions

A.B.: Investigation, Data Curation, Visualization, Writing—Original Draft. A.J.: Investigation, Data Curation, Visualization, Writing—Original Draft. K.O.: Investigation, Writing—Review and Editing. G.E.: Investigation. A.G.: Investigation. T.A.: Investigation. F.K.: Investigation. J.M.: Investigation. R.M.A.: Writing—review and editing, Funding Acquisition. Z.F.R.: Investigation. K.D.: Writing—Review and Editing, Supervision,

Conceptualization, Methodology, Formal Analysis, Funding Acquisition.

Notes

The authors declare no competing financial interest.

■ ACKNOWLEDGMENTS

The authors highly acknowledge the joint financial support from the Czech Science Foundation (project no. GF21-45648L) and the National Centre of Science (NCN) Krakow, Poland, grant OPUS-LAP (2020/39/I/ST4/02039). The authors are grateful to Veronika Kyselová and Lenka Polívková (both from the Department of Sustainable Fuels and Green Chemistry, UCT Prague) for IPA-TPD experiments and Andrey Smirnov (Technopark UCT, Kralupy nad Vltavou) for performing several catalytic tests. F.R.-Z. thanks the Slovenian Research Agency (ARRS) program P2-0393.

■ REFERENCES

(1) Kunkes, E. L.; et al. Catalytic conversion of biomass to monofunctional hydrocarbons and targeted liquid-fuel classes. *Science* **2008**, *322* (5900), 417−421.
(2) Wang, Y.; et al. Efficient and selective conversion of hexose to 5-hydroxymethylfurfural with tin−zirconium-containing heterogeneous catalysts. *Catal. Commun.* **2014**, *50*, 38−43.
(3) Fulignati, S.; Antonetti, C.; Tabanelli, T.; Cavani, F.; Raspolli Galletti, A. M. Integrated Cascade Process for the Catalytic Conversion of 5-Hydroxymethylfurfural to Furanic and TetrahydrofuranicDiethers as Potential Biofuels. *ChemSuschem* **2022**, *15* (13), No. e202200241.
(4) Galkin, K. I.; Ananikov, V. P. Towards Improved Biorefinery Technologies: 5-Methylfurfural as a Versatile C6 Platform for Biofuels Development. *ChemSuschem* **2019**, *12* (1), 185−189.
(5) Post, C.; Maniar, D.; Voet, V. S. D.; Folkersma, R.; Loos, K. Biobased 2,5-Bis(hydroxymethyl)furan as a Versatile Building Block for Sustainable Polymeric Materials. *ACS Omega* **2023**, *8* (10), 8991−9003.
(6) Cui, Y.; Deng, C.; Fan, L.; Qiu, Y.; Zhao, L. Progress in the biosynthesis of bio-based PET and PEF polyester monomers. *Green Chem.* **2023**, *25* (15), 5836−5857.
(7) Kashyap, P.; Jędrzejczyk, M.; Akhgar, M.; Aubrecht, J.; Kubička, D.; Keller, N.; Ruppert, A. Ru/TiO2 Catalyzed High-Yield Synthesis of Furanic Diols by 5-Hydroxymethylfurfural Hydrogenation with Switchable Selectivity. *ChemCatchem* **2025**, *17* (2), No. e202401433.
(8) Ruppert, A. M.; Jędrzejczyk, M.; Sneka-Płatek, O.; Keller, N.; Dumon, A. S.; Michel, C.; Sautet, P.; Grams, J. Ru catalysts for levulinic acid hydrogenation with formic acid as a hydrogen source. *Green Chem.* **2016**, *18* (7), 2014−2028.
(9) Seretis, A.; Diamantopoulou, P.; Thanou, I.; Tzevelekidis, P.; Fakas, C.; Lilas, P.; Papadogianakis, G. Recent Advances in Ruthenium-Catalyzed Hydrogenation Reactions of Renewable Biomass-Derived Levulinic Acid in Aqueous Media. *Front. Chem.* **2020**, *8*, 221.
(10) Kim, A.; Sanchez, C.; Patriarche, G.; Ersen, O.; Moldovan, S.; Wisnet, A.; Sassoye, C.; Debecker, D. P. Selective CO 2 methanation on Ru/TiO 2 catalysts: unravelling the decisive role of the TiO 2 support crystal structure. *Catal. Sci. Technol.* **2016**, *6* (22), 8117−8128.
(11) Fulignati, S.; et al. Insight into the hydrogenation of pure and crude HMF to furan diols using Ru/C as catalyst.Applied Catalysis A. *General* **2019**, *578*, 122−133.
(12) Hernandez-Mejia, C.; Gnanakumar, E. S.; Olivos-Suarez, A.; Gascon, J.; Greer, H. F.; Zhou, W.; Rothenberg, G.; Raveendran Shiju, N. Ru/TiO 2-catalysed hydrogenation of xylose: the role of the crystal structure of the support. *Catal. Sci. Technol.* **2016**, *6* (2), 577−582.
(13) Aubrecht, J.; et al. Unveiling the intrinsic activity of TiO2 in HMF valorisation. *Chem. Eng. J.* **2024**, *498*, 155867.
(14) Rodríguez-Padrón, D.; Perosa, A.; Longo, L.; Luque, R.; Selva, M. Tuning the Selectivity of the Hydrogenation/Hydrogenolysis of 5-Hydroxymethylfurfural under Batch Multiphase and Continuous-Flow Conditions. *ChemSuschem* **2022**, *15* (13), No. e202200503.
(15) Fulignati, S.; Antonetti, C.; Wilbers, E.; Licursi, D.; Heeres, H. J.; Raspolli Galletti, A. M. Tunable HMF hydrogenation to furan diols in a flow reactor using Ru/C as catalyst. *J. Ind. Eng. Chem.* **2021**, *100*, 390.e1−390.e9.
(16) Dong, L.; et al. Selective hydrogenolysis of 5-hydroxymethylfurfural to 5-methylfurfural over Au/TiO2.Applied Catalysis B. *Environmental* **2023**, *335*, 122893.
(17) Li, S.; Dong, M.; Yang, J.; Cheng, X.; Shen, X.; Liu, S.; Wang, Z.-Q.; Gong, X.-Q.; Liu, H.; Han, B. Selective hydrogenation of 5-(hydroxymethyl)furfural to 5-methylfurfural over single atomic metals anchored on Nb2O5. *Nat. Commun.* **2021**, *12* (1), 584.
(18) Liu, J.-L.; et al. Ce-promoted Ru/SBA-15 catalysts prepared by a "two solvents" impregnation method for selective hydrogenation of benzene to cyclohexene.Applied Catalysis A. *General* **2009**, *353* (2), 282−287.
(19) Mazzieri, V.; et al. XPS, FTIR and TPR characterization of Ru/Al2O3 catalysts. *Appl. Surf. Sci.* **2003**, *210* (3), 222−230.
(20) Crawford, J. M.; et al. Influence of residual chlorine on Ru/TiO2 active sites during CO2 methanation.Applied Catalysis A. *General* **2023**, *663*, 119292.
(21) Liu, Y.; et al. Conversion of glucose to levulinic acid and upgradation to γ-valerolactone on Ru/TiO2 catalysts. *New J. Chem.* **2021**, *45* (32), 14406−14413.
(22) Tike, M. A.; Mahajani, V. V. Kinetics of Liquid-Phase Hydrogenation of Furfuryl Alcohol to Tetrahydrofurfuryl Alcohol over a Ru/TiO2 Catalyst. *Ind. Eng. Chem. Res.* **2007**, *46* (10), 3275−3282.
(23) Bergeret, G.; Gallezot, P.; Particle Size and Dispersion Measurements. In *Handbook Of Heterogeneous Catalysis*; Wiley, pp. 738−765.
(24) Fairley, N.; et al. Systematic and collaborative approach to problem solving using X-ray photoelectron spectroscopy. *Appl. Surf. Sci. Adv.* **2021**, *5*, 100112.
(25) Mo, S.-D.; Ching, W. Electronic and optical properties of three phases of titanium dioxide: Rutile, anatase, and brookite. *Phys. Rev. B* **1995**, *51* (19), 13023.
(26) Al-Oubidy, E. A.; Kadhim, F. J. Photocatalytic activity of anatase titanium dioxide nanostructures prepared by reactive magnetron sputtering technique. *Opt. Quant. Electron.* **2019**, *51* (1), 23.
(27) Swain, J. E.; et al. Characterization of titania surface area in titania/silica SCR catalysts by temperature-programmed reaction of 2-propanol. *Appl. Catal., A* **1996**, *139* (1), 175−187.
(28) Kulkarni, A. P.; Muggli, D. S. The effect of water on the acidity of TiO2 and sulfated titania. Applied Catalysis A. *General* **2006**, *302* (2), 274−282.
(29) Cai, W.; et al. Ruthenium/titanium oxide interface promoted electrochemical nitrogen reduction reaction. *Chem. Catal.* **2022**, *2* (7), 1764−1774.
(30) Morgan, D. J. Resolving ruthenium: XPS studies of common ruthenium materials. Surface and Interface Analysis. *Surf. Interface Anal.* **2015**, *47* (11), 1072−1079.
(31) Grey, L. H.; Nie, H.-Y.; Biesinger, M. C. Defining the nature of adventitious carbon and improving its merit as a charge correction reference for XPS. *Appl. Surf. Sci.* **2024**, *653*, 159319.
(32) Zhao, Y.; et al. Ruthenium oxychloride supported by manganese oxide for stable oxygen evolution in acidic media. *J. Mater. Chem. A* **2022**, *10* (39), 20964−20974.
(33) Kashyap, P.; Jędrzejczyk, M.; Akhgar, M.; Aubrecht, J.; Kubička, D.; Keller, N.; Ruppert, A. Ru/TiO2 Catalyzed High-Yield Synthesis of Furanic Diols by 5-Hydroxymethylfurfural Hydrogenation with Switchable Selectivity. *ChemCatChem* **2025**, *17*, No. e202401433.
(34) Kim, H.; Park, J. H.; Ha, J.-M.; Kim, D. H. Effect of Hydrogen Spillover on the Ru/TiO2-Catalyzed Guaiacol Hydrodeoxygenation: Rutile vs Anatase TiO2. *ACS Catal.* **2023**, *13* (18), 11857−11870.
(35) Pintar, A.; Batista, J.; Tišler, T. Catalytic wet-air oxidation of aqueous solutions of formic acid, acetic acid and phenol in a continuous-flow trickle-bed reactor over Ru/TiO2 catalysts. *Appl. Catal., B* **2008**, *84* (1), 30−41.

(36) Lanza, R.; Järås, S. G.; Canu, P. Partial oxidation of methane over supported ruthenium catalysts. Applied Catalysis A. *General* **2007**, *325* (1), 57−67.
(37) Camposeco, R.; et al. Highly active Ru/TiO2 nanostructures for total catalytic oxidation of propane. *Environ. Sci. Pollut. Res.* **2023**, *30* (43), 98076−98090.
(38) Mazzieri, V. A.; L'Argentière, P. C.; Coloma-Pascual, F.; Fígoli, N. S. Effect of Chlorine on the Properties of Ru/Al2O3. *Ind. Eng. Chem. Res.* **2003**, *42* (11), 2269−2272.
(39) Pinzón, M.; et al. Hydrogen production by ammonia decomposition over ruthenium supported on SiC catalyst. *J. Ind. Eng. Chem.* **2021**, *94*, 326−335.
(40) Nagpure, A. S.; Venugopal, A. K.; Lucas, N.; Manikandan, M.; Thirumalaiswamy, R.; Chilukuri, S. Renewable fuels from biomass-derived compounds: Ru-containing hydrotalcites as catalysts for conversion of HMF to 2, 5-dimethylfuran. *Catal. Sci. Technol.* **2015**, *5* (3), 1463−1472.
(41) Mishra, D. K.; Lee, J.-M.; Chang, J.-S.; Hwang, J.-S. Liquid phase hydrogenation of d-glucose to d-sorbitol over the catalyst (Ru/NiO−TiO2) of ruthenium on a NiO-modified TiO2 support. *Catal. Today* **2012**, *185* (1), 104−108.
(42) Fontana, J.; et al. Evaluation of some supports to RuSn catalysts applied to dimethyl adipate hydrogenation. *Catal. Today* **2011**, *172* (1), 27−33.
(43) Wismeijer, A.; Kieboom, A.; Van Bekkum, H. Selective hydrogenation of citronellal to citronellol over Ru/TiO2 as compared to Ru/SiO2. *Appl. Catal* **1986**, *25* (1−2), 181−189.
(44) Tolek, W.; Nanthasanti, N.; Pongthawornsakun, B.; Praserthdam, P.; Panpranot, J. Effects of TiO2 structure and Co addition as a second metal on Ru-based catalysts supported on TiO2 for selective hyd rogenation of furfural to FA. *Sci. Rep.* **2021**, *11* (1), 9786.
(45) Hadjiivanov, K.; et al. FTIR Study of CO Interaction with Ru/TiO2Catalysts. *J. Catal.* **1998**, *176* (2), 415−425.
(46) Guglielminotti, E.; Bond, G. C. Effect of oxidation−reduction treatments on the infrared spectra of carbon monoxide chemisorbed on a Ru/TiO2 catalyst. *J. Chem. Soc., Faraday Trans.* **1990**, *86* (6), 979−987.
(47) Zhang, Y.; et al. Ru/TiO2 Catalysts with Size-Dependent Metal/Support Interaction for Tunable Reactivity in Fischer−Tropsch Synthesis. *ACS Catal.* **2020**, *10* (21), 12967−12975.
(48) Martra, G. Lewis acid and base sites at the surface of microcrystalline TiO2 anatase: relationships between surface morphology and chemical behaviour. Applied Catalysis A. *General* **2000**, *200* (1−2), 275−285.
(49) Turkin, A.; et al. How Trace Impurities Can Strongly Affect the Hydroconversion of Biobased 5-Hydroxymethylfurfural? *ACS Catal.* **2021**, *11* (15), 9204−9209.
(50) Yang, Y.; et al. Selective hydrodeoxygenation of 5-hydroxymethylfurfural to 2, 5-dimethylfuran on Ru−MoO x/C catalysts. *RSC Adv.* **2017**, *7* (27), 16311−16318.
(51) Dong, Z.; Zhang, Y.; Xia, H. Selective hydrogenolysis of 5-hydroxymethylfurfural to 2, 5-dimethylfuran with high yield over bimetallic Ru−Co/AC catalysts. *RSC Adv.* **2024**, *14* (21), 14982−14991.
(52) Galvagno, S.; et al. Hydrogenation of cinnamaldehyde over Ru/C catalysts: effect of Ru particle size. *J. Mol. Catal.* **1991**, *64* (2), 237−246.
(53) Newman, C.; et al. Effects of support identity and metal dispersion in supported ruthenium hydrodeoxygenation catalysts. Applied Catalysis A. *General* **2014**, *477*, 64−74.
(54) Ochoa, A.; Aramburu, B.; Valle, B.; Resasco, D. E.; Bilbao, J.; Gayubo, A. G.; Castaño, P. Role of oxygenates and effect of operating conditions in the deactivation of a Ni supported catalyst during the steam reforming of bio-oil. *Green Chem.* **2017**, *19* (18), 4315−4333.
(55) Duarte, D. P.; Martínez, R.; Hoyos, L. J. Hydrodeoxygenation of 5-Hydroxymethylfurfural over Alumina-Supported Catalysts in Aqueous Medium. *Ind. Eng. Chem. Res.* **2016**, *55* (1), 54−63.

https://doi.org/10.1021/acssuschemeng.5c04908
ACS Sustainable Chem. Eng. 2025, 13, 11652−11667